HHS Public Access

Author manuscript

Cell Rep. Author manuscript; available in PMC 2024 December 04.

Published in final edited form as:

Cell Rep. 2024 October 22; 43(10): 114860. doi:10.1016/j.celrep.2024.114860.

Comprehensive mapping of sensory and sympathetic innervation of the developing kidney

Pierre-Emmanuel Y. N'Guetta[1], **Sarah R. McLarnon**[1], **Adrien Tassou**[1,2,3], **Matan Geron**[1,2,3], **Sepenta Shirvan**[4], **Rose Z. Hill**[4], **Grégory Scherrer**[1,2,3], **Lori L. O'Brien**[1,5,6,*]

[1]Department of Cell Biology and Physiology, The University of North Carolina at Chapel Hill, Chapel Hill, NC 27599, USA

[2]UNC Neuroscience Center, The University of North Carolina at Chapel Hill, Chapel Hill, NC 27599, USA

[3]Department of Pharmacology, The University of North Carolina at Chapel Hill, Chapel Hill, NC 27599, USA

[4]Department of Neuroscience, Dorris Neuroscience Center, The Scripps Research Institute, La Jolla, CA 92037, USA

[5]UNC Kidney Center, The University of North Carolina at Chapel Hill, Chapel Hill, NC 27599, USA

[6]Lead contact

SUMMARY

The kidneys act as finely tuned sensors to maintain physiological homeostasis. Both sympathetic and sensory nerves modulate kidney function through precise neural control. However, how the kidneys are innervated during development to support function remains elusive. Using light-sheet and confocal microscopy, we generated anatomical maps of kidney innervation across development. Kidney innervation commences on embryonic day 13.5 (E13.5) as network growth

*Correspondence: lori_obrien@med.unc.edu.

AUTHOR CONTRIBUTIONS

L.L.O. conceptualized the study, supervised research, guided experiments, interpreted data, helped assemble figures, and revised the manuscript. P.-E.Y.N. performed experiments, analyzed data, assembled figures, and wrote the manuscript. S.R.M. performed mouse surgery for retrograde tracing and contributed to the PIEZO2 experiments and analyses. A.T. helped inject mice for the retrograde tracing. A.T. and M.G. dissected, imaged, and analyzed DRG data. G.S. interpreted retrograde tracing data and supervised A.T.'s and M.G.'s research. R.Z.H. performed NFH, NPY/TH, and CGRP/TH immunostaining, interpreted the results, assembled the associated figures, and supervised S.S. S.S. immunostained and quantified CGRP/TH innervation of glomeruli. All authors contributed to the manuscript text relevant to their contributions.

DECLARATION OF INTERESTS

The authors declare no competing interests.

SUPPLEMENTAL INFORMATION

Supplemental information can be found online at https://doi.org/10.1016/j.celrep.2024.114860.

RESOURCE AVAILABILITY

Lead contact

Requests for resources, reagents, and further information should be directed to the lead contact, Lori O'Brien (lori_obrien@med.unc.edu).

Materials availability

This study did not generate new or unique reagents.

Data and code availability

Imaging files are publicly available on the UNC Dataverse: https://dataverse.unc.edu/dataverse/D_24_01486_obrienlab.

aligns with arterial differentiation. Fibers are synapsin I^+, highlighting ongoing axonogenesis and potential signaling crosstalk. By E17.5, axons associate with nephrons, and the network continues to expand postnatally. $CGRP^+$, substance P^+, $TRPV1^+$, and $PIEZO2^+$ sensory fibers and TH^+ sympathetic fibers innervate the developing kidney. TH^+ and $PIEZO2^+$ axons similarly innervate the human kidney, following the arterial tree to reach targets. Retrograde tracing revealed the primary dorsal root ganglia, T10–L2, from which sensory neurons project to the kidneys. Together, our findings elucidate the temporality and neuronal diversity of kidney innervation.

Graphical Abstract

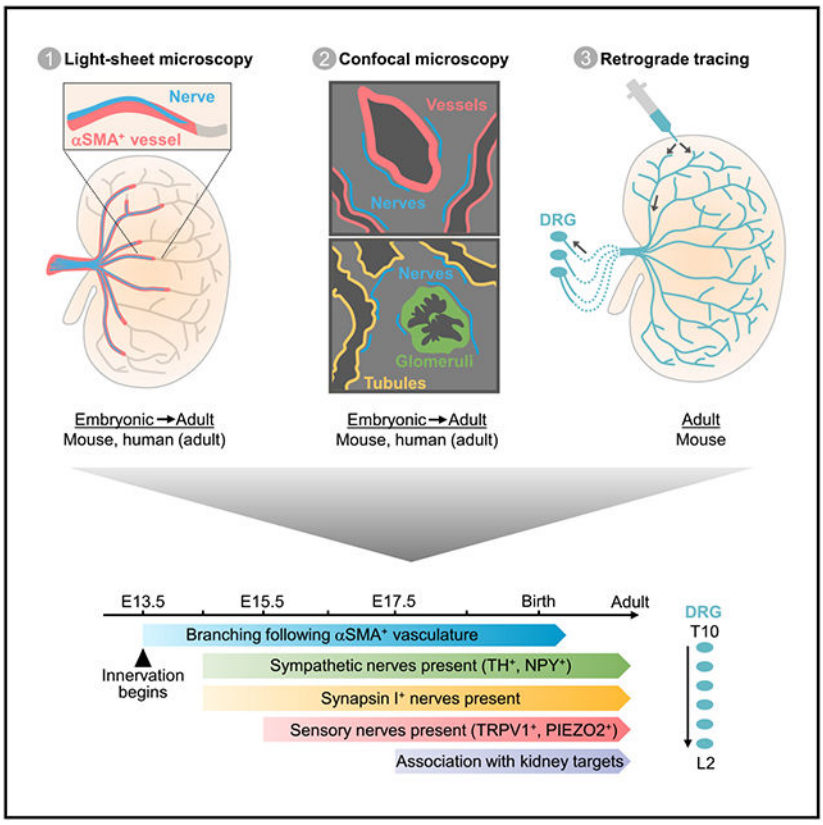

In brief

N'Guetta et al. map the spatiotemporal innervation of the developing mouse kidney. They find that innervation begins at E13.5 and that this network expands with the arterial tree. Sympathetic and sensory nerves associate with nephrons by E17.5, maintaining these associations into adulthood with similar innervation patterns found in the human kidneys.

INTRODUCTION

Major functions of the kidneys include maintenance of body fluid and electrolyte homeostasis and modulation of blood pressure. These functions are maintained by a variety of intrinsic cellular mechanisms as well as extrinsic input from the nervous system.[1-3] Peripheral neurons originating from external ganglia innervate the kidneys and

are predominantly unmyelinated C-fibers.[3-7] These nerves are classified as afferent sensory neurons that influence cardiovascular function through the relay of chemical and mechanical information from the kidneys to the central nervous system (CNS) or efferent sympathetic neurons that regulate renal function through the CNS.[3] Precise innervation and modulation of nerve activity maintains kidney physiology, while aberrant nerve function is associated with several kidney diseases.[8-10] Therefore, modulating nerve activity is widely seen as a potential therapy to address kidney-related physiological disorders.[11] Yet, to achieve such precise neuromodulation, an accurate mapping of the kidney nerve origins and a complete understanding of their molecular identity are necessary. Many studies to date have focused on sympathetic nerves and their regulation of mature kidney physiology. Therefore, we still lack detailed information about how both the sensory and sympathetic innervation of the kidneys is established and how nerves pattern to reach their target cells and establish crosstalk.

Sympathetic nerves help control kidney vascular tone, glomerular filtration rate, sodium and water reabsorption, and renin release.[12-14] They also modulate processes such as cytokine release to mediate inflammatory responses.[3,15-17] However, increased renal sympathetic nerve activity contributes to the development and maintenance of hypertension, and overactivity is common in chronic kidney disease.[3,10,18] In contrast, the full complement and organization of kidney sensory nerves as well as their normal and pathophysiological roles remains poorly understood.[3] Kidney sensory nerves have thus far been classified as transient receptor potential cation channel subfamily V member 1-positive ($TRPV1^+$) due to their response to capsaicin. They have also been shown to produce the nociceptor-associated neuropeptides calcitonin gene-related peptide (CGRP) and substance P.[3,19] Sensory neurons innervating the kidneys project to the dorsal horn and synapse onto interneurons that project to CNS sites regulating cardiovascular function and, in turn, feed back to modulate kidney sympathetic nerve activity.[20] Recently, studies have established the importance of mechanosensitive PIEZO2 sensory nerves in the urogenital system to regulate bladder and sexual function.[21,22] However, whether PIEZO2 sensory nerves also innervate the kidney is unknown. Lastly, a recent study published by Cheng et al. has shown parasympathetic cholinergic (choline $acetyltransferase^+$ and vesicular acetylcholine transporter $[VAChT]^+$) nerves innervate the renal artery and pelvis with cholinergic ganglia found within the kidney nerve plexus.[23] Whether these axons project to the kidney cortex and associate with structures within the kidneys has not been elucidated to date. Renal denervation is a promising option for the treatment of primary hypertension, although not all patients benefit from the procedure.[24-29] Understanding the full extent of kidney innervation and nerve activity may inform efforts to optimize such strategies.

Ganglia located externally send axonal projections to the kidneys. Axons navigate along the renal artery, and recent studies report the close association of nerves with the developing kidney arterial tree.[30,31] Depending on the model system, sympathetic innervation arises from the celiac, superior mesenteric, and aorticorenal ganglia and partially from the paravertebral chain.[32-36] In rats, studies have shown that kidney sensory neurons project from dorsal root ganglia (DRG) at spinal levels T6–L4, the majority of which derive from T12–L3.[37,38] However, the origin of sensory axons that innervate the mouse kidneys is unclear. Moreover, the process of kidney innervation during development, in any model,

has not been detailed thoroughly. To this end, we mapped the spatiotemporal innervation of the mouse kidneys from embryonic to early postnatal development. We establish when kidney innervation begins, its origins in the DRG, the spatial organization and growth of axons, their association with kidney cells and structures, as well as the identity of the nerves across these different stages. Additionally, we validated their associations and identity in both mouse and human adult kidney tissue. Altogether, we generated a rich resource of knowledge surrounding kidney innervation that will inform studies of both kidney development and physiological regulation.

RESULTS

Spatiotemporal mapping of kidney innervation

We set out to determine when neuronal axons first reach the kidneys and how this network subsequently expands. We generated spatiotemporal maps of kidney innervation by performing whole-mount immunostaining followed by 3D light-sheet imaging of either whole urogenital systems (UGSs; embryonic day 12.5 [E12.5] and E13.5) or individual kidneys (E14.5, E16.5, E18.5, postnatal day 0 [P0], and P7). Tissues were immunostained with the pan-neuronal marker β-tubulin class III (TUBB3) to visualize axons, the arterial marker α-smooth muscle actin (αSMA), and the endothelial marker CD31. Male and female kidneys were both examined, with no significant differences observed; therefore, the data presented are representative of either sex. At E12.5, kidneys were discerned by cytokeratin staining of the ureteric tree; however, no $TUBB3^+$ nerves could be identified in the kidneys (Figure 1A; Video S1). αSMA^+ cells were primarily localized to the descending aorta and not yet found in the kidneys, correlating with previous investigations of kidney vascularization.[39] Despite the lack of axons in the kidneys, we observed ganglia and postganglionic nerve fibers tracking with the descending aorta (Figure 1A). As organogenesis continues, $TUBB3^+$ nerve fibers navigate toward the kidneys and begin innervation at E13.5, closely associating with αSMA^+ mural cells, which mark the maturing renal arteries (Figure 1B; Videos S2 and S3).[30,31,39,40] Despite the low αSMA^+ mural cell coverage at this time point, an extensive $CD31^+$ endothelial network is established by E13.5 (Figure 1B; Video S3).

At E14.5, αSMA coverage was more extensive, marking several arterial branches (Figure S1A). Concurrently, $TUBB3^+$ nerve fibers continue tracking with the major arterial branches, only extending along the portion of endothelium with αSMA^+ mural cell coverage. Additionally, axons track with the αSMA^+ ureteric smooth muscle layer (Figure S1A). As development continues, axons grow and branch in coordination with the arterial network as the major branches are established by E16.5 (Figure 1C; Video S4). Multiple nerve fibers associate with a single arterial branch, and these larger fibers consist of multiple axons that are tightly bundled (Figure 1C). Subsequently, the axonal network expanded via interstitial branching, as observed at E18.5. The branching axons loop around structures such as glomeruli (Figure 1D; Video S5). Subsequent imaging of the postnatal kidney at P0 (Figure S1B) and P7 (Figure S1C) revealed a significant increase in nerve fiber density and arborization of the network due to continued axonal growth and branching.

To visualize the innervation of target cells and structures at greater resolution, we performed confocal imaging on E18.5 kidney sections. Supporting our whole-mount 3D analyses, we observed axons tightly associating with αSMA$^+$ vasculature (Figure S1D). Nerves track with renal arteries and arterioles into the cortex and dissociate from the αSMA$^+$ mural cells to loop around and associate with the Bowman's capsule of glomeruli (Figures 1D and S1E) and tubule epithelia (Figure S1F).

Sensory nerves innervate the developing kidneys

While we mapped kidney innervation across several developmental time points, TUBB3 is a pan-neuronal marker and cannot discern between sensory or sympathetic fibers. To visualize the distribution and abundance of sensory neurons in the developing kidneys, we crossed the *Trpv1^{Cre}* line to the *Rosa(R)26^{tdTomato}* reporter line (*Trpv1$^{Cre/+}$;R26$^{tdTomato/+}$*) to label all nociceptive TRPV1$^+$ neurons. TRPV1$^+$ nociceptive neurons are thought to comprise the majority of, if not all, sensory nerves within the mature kidney, and, therefore, labeling this population should highlight the sensory contribution.[19,41] We performed wholemount imaging on E16.5 *Trpv1$^{Cre/+}$;R26$^{tdTomato/+}$* kidneys to visualize the total complement of sensory nerve fibers traced from the start of kidney innervation. The tdTomato$^+$ signal overlapped extensively with TUBB3 (Figure 2A). Sections from P1 *Trpv1$^{Cre/+}$;R26$^{tdTomato/+}$* kidneys show tdTomato$^+$ nerve fibers adjacent to LRP2$^+$ proximal tubules and E-cadherin (ECAD)$^+$ epithelial structures (Figure 2B). Additionally, tdTomato$^+$ axons are found adjacent to arteries, arterioles, and glomeruli (Figure 2C).

Nociceptive sensory afferent nerve identity and function can also be defined by the production of neuropeptides such as CGRP and substance P. To assess renal peptidergic sensory innervation, we examined kidney sections at E14.5, E15.5, E18.5, P0, and adult stages, immunostained for CGRP and substance P. We validated the specificity of CGRP and substance P antibodies for sensory neurons on isolated DRG and superior cervical ganglion (SCG) tissue sections. As expected, sensory ganglia showed extensive CGRP and substance P labeling, while sympathetic SCG showed no positive signal (Figures S2A and S2B). At E14.5, we could not yet detect CGRP$^+$ or substance P$^+$ nerves in the kidney (Figures S2C and S2D). However, by E15.5, we observed CGRP$^+$ sensory nerves that closely associated with renal arteries (Figure 3A). These CGRP$^+$ fibers were also TRPV1 (tdTomato$^+$) sensory fibers (Figure S2E). To circumvent cross-reactivity issues due to several of our antibodies being raised in the same species, we crossed the transgenic podocin Cre line (Pod-Cre^{tg}) to the *R26^{tdTomato}* reporter (Pod-Cre$^{tg/+}$*;R26$^{tdTomato/tdTomato}$*), thereby labelling glomerular podocytes with tdTomato. Assessing the kidneys of these animals at P0, we found CGRP$^+$ nerves near glomeruli and proximal tubules (Figure 3B). In adult kidneys, CGRP$^+$ fibers are similarly associated with the vasculature and Bowman's capsule (Figure 3C). Substance P immunolabelling was detected by E18.5, labeling axons adjacent to blood vessels and glomeruli (Figure 3D), with similar localization observed in adult kidneys (Figure 3E). Peripheral neurons innervating the kidneys are predominantly unmyelinated C-fibers, although it has been suggested that some myelinated afferent fibers are present in the kidneys.[3-7] However, it was unclear whether these fibers were peptidergic. To address this, we assessed the colocalization of CGRP$^+$ fibers and neurofilament heavy polypeptide (NFH), a component of large-diameter myelinated axons, in adult kidneys (Figure S2F).

In the kidney cortex, a few NFH^+ fibers were observed, although they did not come in proximity to glomeruli, and the CGRP signal did not overlap with the fibers. In the renal pelvis, we observed minor overlap of NFH and CGRP along the pelvic urothelium (Figure S2F), supporting the presence, although sparse, of myelinated peptidergic sensory fibers within the kidneys.

PIEZO2 is a mechanoreceptor utilized by a subset of peripheral sensory neurons, including those that innervate the bladder to help coordinate urination and genital sub-regions to support sexual function.[21,22,42] We investigated whether PIEZO2 neurons also innervate the kidneys. Whole-mount immunostaining at E18.5 revealed $PIEZO2^+$ axons overlapping with the $TUBB3^+$ network (Figure S2G). Further analysis of kidney sections showed that $PIEZO2^+$ neurons primarily associate with large vessels earlier in development (Figure 3F) and, by P0, are found adjacent to glomeruli and proximal tubules (Figure 3G).

Retrograde tracing identifies the DRG origin of kidney sensory neurons

The somata of peripheral sensory neurons are located in DRG present along the spinal column. To identify the DRG that contain sensory neurons projecting to the kidneys, we performed retrograde tracing experiments. The fluorescently labeled neuronal tracer cholera toxin subunit B (CTB) was injected into the right kidney cortex (ipsilateral) of adult mice. Four days after the injection, both the injected and non-injected kidney (contralateral) as well as the ipsilateral and contralateral DRG were dissected to determine the origin of kidney sensory innervation (Figure 4A). By examining the fluorescent signal from all cervical, thoracic, lumbar, and sacral DRG, we determined that kidney sensory innervation traces to the ipsilateral DRG of the lower thoracic (T10–T13), lumbar (L1–L6), and sacral (S1–S2) regions, with the majority of sensory innervation projecting from the lower thoracic (T10–T13) and upper lumbar (L1–L2) regions (Figures 4B and 4D). Ipsilateral kidney sections showed CTB^+ nerves near vasculature and glomeruli (Figure 4C). Strikingly, we observed CTB^+ cells within the contralateral DRG of the upper lumbar region (L1–L2), suggesting that these DRG may also innervate the ipsilateral kidney (Figure 4B). Additionally, we observed a few CTB^+ nerve fibers around blood vessels in the contralateral kidney (Figure 4C). No difference was identified between male and female mice in the tracing results obtained.

Next, we specifically traced $PIEZO2^+$ sensory neurons using pAAV-FLEX-tdTomato packaged with AAV-PHP.S (AAV-PHP.S:FLEX-tdTomato) injected into the right kidney of *Piezo2*$^{EGFP\text{-}IRES\text{-}Cre/+}$ mice (Figure S3A). The FLEX vector contains a floxed tdTomato sequence enabling Cre-mediated reporter expression, while AAV-PHP.S transduces peripheral neurons.[43] The tracing confirmed innervation of the kidney by $PIEZO2^+$ mechanosensory neurons, with the majority of $PIEZO2^+$ nerves projecting from the lower thoracic (T10, T12, and T13) and lumbar (L1 and L2) DRG (Figures S3B and S3C).

Sympathetic and cholinergic innervation of the developing kidneys

Sympathetic postganglionic neurons produce tyrosine hydroxylase (TH), an enzyme involved in catecholamine synthesis, and this marker has been utilized previously in adult kidneys to localize sympathetic nerves.[44,45] Thus, to determine the distribution of

sympathetic nerves in developing kidneys, we performed whole-mount immunolabeling with a TH antibody (Figures 5A and 5B). At E14.5, TH^+ fibers were detected in the kidneys, overlapping with TUBB3 and tracking with the arteries (Figure 5A). By P0, the sympathetic nerves had branched significantly with the arterial tree, and TH^+ axons were found navigating around $LRP2^+$ proximal tubules (Figure 5B). We also examined kidney sections and similarly observed TH^+ axons primarily associated with renal arteries at earlier stages of development (Figure 5C). By P0, the nerves could be found abutting glomeruli and proximal tubules (Figure 5D). A small proportion of sensory nerves express and produce TH.[46,47] We confirmed isolated adult DRG contain TH^+ somata; however, they constitute only a minor proportion of sensory neurons (Figure S4A). We further validated sympathetic nerve identity by co-immunostaining adult kidney sections with the sympathetic marker neuropeptide Y (NPY) and TH. All NPY^+ fibers examined, such as those adjacent to glomeruli, were TH^+, supporting their sympathetic identity (Figure 5E). We also investigated the overlap of TH^+ and $CGRP^+$ fibers and found them co-associating with glomeruli and in the renal pelvis (Figure S4B). We then quantified the percentage of glomeruli that were innervated by either TH^+ fibers, $CGRP^+$ fibers, or both. A previous study performed similar quantitation and found $CGRP^+$ fibers associated with ~48% of glomeruli in wild-type adult mice.[19] Corroborating these findings, our analyses identified that 40% of glomeruli were associated with $CGRP^+$ fibers. TH^+ axons associated with 50% of glomeruli, and ~37% were innervated by both $CGRP^+$ and TH^+ axons (Figure S4C).

Previous studies showed that, during development, TH may be produced by cholinergic parasympathetic nerves.[48] NPY also labels a subset of cholinergic pelvic ganglia.[49,50] A recent study has demonstrated parasympathetic innervation of the main renal artery and pelvis, but there is no anatomic evidence of significant parasympathetic innervation into the kidneys. To determine whether there are cholinergic nerves in the kidneys, we immunostained P0 and adult kidney sections for the cholinergic marker VAChT. We validated the specificity of the VAChT antibody on several P0 tissues. The bladder, which is primarily innervated by parasympathetic neurons, contained $VAChT^+$ axons (Figure S5A).[51] Sympathetic aorticorenal ganglia through which parasympathetic fibers pass were also positive for VAChT, although the signal did not show significant overlap with TUBB3 in the soma (Figure S5A). The P0 kidney cortex contained sparse $VAChT^+$ fibers that overlapped with TUBB3 near large vessels (Figure S5A). In the adult kidneys, $VAChT^+$ fibers were similarly sparse compared to NPY^+ sympathetic nerves, and the VAChT signal did not show direct overlap with NPY, suggesting that different fibers are present in the same bundle (Figure S5B). In relation to kidney structures, $VAChT^+$ axons were observed around the vasculature, tubules, and glomeruli, suggesting that parasympathetic fibers can innervate the kidneys past the main renal artery (Figures S5C and S5D).

Evidence for the establishment of neuroeffector junctions during kidney development

In order to have an impact on kidney development and physiology, neurons need to establish functional crosstalk with kidney cells. To investigate the formation of neuroeffector junctions, synapse-like structures that form between neurons and non-neuronal cells, we characterized the cellular localization of a synaptic marker. Using an antibody raised against synapsin I (SYN1), a membrane-associated phosphoprotein contained within small

synaptic vesicles of presynaptic nerves, we investigated whether and at which stage SYN1 is detected. At E14.5 and E16.5, $SYN1^+$ axons were primarily observed around the $CD31^+$ vasculature (Figure 6A). By P0, $SYN1^+$ axons were also identified near proximal tubules and glomeruli (Figure 6B). A similar pattern was retained in the adult, with $SYN1^+$ axons found along the vasculature and adjacent to glomeruli (Figure 6C).

Next, we investigated the developmental expression of receptors associated with various neuronal signaling mechanisms and known postsynaptic markers to understand which kidney cells are responsive to neuronal signaling. We utilized a publicly available single-cell RNA sequencing (scRNA-seq) dataset from E18.5 kidneys to obtain the enrichment of these factors in the various cells of the developing kidneys.[52] We found that a variety of cell types and structures, including nephron progenitors, stromal cells, renal vesicles, and the S-shaped body, express the α-adrenergic receptors *Adra1a* and *Adra1b*, whereas *Adra2a* and *Adra2b* were enriched in the distal tubules, ureteric epithelium, and proximal tubules (Figure S6A). We also noted that the β-adrenergic receptor *Adrb2* was strongly enriched in the resident immune cells, while *Adrb3* was expressed by stromal cells (Figure S6A). Next, we also looked for the expression of major purinergic receptors in the developing kidneys. Many of the ATP and adenosine receptors, including *P2rx4*, *P2rx7*, *P2ry6*, *P2yr12*, *P2yr13*, *P2yr14*, *Lpar6*, and *Lpar4*, showed enrichment in the resident immune cells. Endothelial cells, tubule epithelium, and ureteric epithelium showed expression of *Ador2a*, *P2ry1*, *Lpar6*, *Lpar4*, and *Adora1*, while *P2rx4* and *P2ry14* were moderately enriched in podocytes (Figure S6B). Last, we observed the enrichment of known post-synaptic markers or synapse-promoting markers like *Vamp2*, *Tenm3*, *Tenm4*, *Ephb1*, *Ephb3*, *Epha2*, and *Grm7* by podocytes; *Nlgn1*, *Epha2*, *Ephb1*, and *Ephb4* by endothelial cells; and *Gria3*, *Ephb2*, *Ephb3*, *Ephb4*, *Ephb6*, *Epha1*, *Epha4*, *Epha7*, *Tenm2*, *Dlg4*, *Dlg1*, and *Nlgn3* by the distal and proximal tubules (Figure S6C).

The spatial organization of nerves is conserved in adult human kidneys

A key difference between mouse and human kidneys is the number of lobes, thus generating differences in vascular organization. Additionally, the latter stages of nephrogenesis in humans occur via arcading and lateral branching, which differ in their organization compared to the mouse.[53] Given the specific distribution of kidney nerves around the vasculature and nephrons in the mouse, we investigated their organization in human kidneys. Whole-mount immunostaining of human kidney cortex tissue with αSMA and podocin highlighted the distinct organization of human cortical nephrons into cluster-like arrangements of glomeruli (Figure 7A; Video S6). Similar to the mouse, TH^+ sympathetic nerves branch following the αSMA vasculature until they reach the cortex. Axons travel along interlobar arteries, which then branch into the arcuate and interlobular arteries (Figure 7B; Video S7). Higher-resolution imaging of human kidney sections shows that these TH^+ fibers loop around glomeruli and tubule epithelium (Figure S7). We also assessed whether PIEZO2 mechanosensory neurons innervate the human kidneys and confirmed that $PIEZO2^+$ nerves were associated with vessels, glomeruli, and the kidney epithelium (Figure 7C). To investigate the signaling competency of these nerves, we assessed synapsin 1 localization. We observed $SYN1^+$ nerve fibers in close association with glomeruli and

tubules (Figure 7D; Video S8). Taken together, these data show that the close association of both sympathetic and sensory nerves with vessels and nephrons is conserved in humans.

DISCUSSION

In this study, we set out to investigate the process of kidney innervation across organogenesis. We generated spatiotemporal maps of innervation using markers specific to various classes of axons and identified the presence of both sensory and sympathetic nerves as well as evidence for parasympathetic innervation. High-resolution imaging of kidney sections revealed the association of nerves with the vasculature, glomeruli, and tubules. A synaptic vesicle marker and scRNA-seq data highlight the potential for nerve-kidney crosstalk during kidney development. Finally, we established that human kidneys show similar associations of sympathetic and sensory nerve subclasses with the vasculature and nephrons. Altogether, we garnered substantial insights into the process of kidney innervation with implications for both development and physiological regulation.

The close association of nerves with kidney vasculature

We established that kidney innervation begins at E13.5 and coincides with arterial differentiation as vascular smooth muscle cells associate with the nascent endothelium. Our findings of a tight association between axons and vascular smooth muscle cells correlates with a recent description of kidney innervation[31] and our own prior studies.[30] This is conserved between mouse and human, with nerves navigating alongside the major human renal arteries. In the developing mouse kidney, it has been shown that arterial differentiation initiates at ~E13.5 and progresses toward the kidney periphery.[39,40] We hypothesize that αSMA^+ mural cells may be signaling to the axons, thereby guiding the nerves as the arteries differentiate and grow. This has been shown in other systems, with axons responding to vascular-derived cues like artemin (*Artn1*), endothelin 3 (*Edn3*), and neurotrophin 3 (*Ntf3*).[54-56] As inferred from E18.5 scRNA-seq, *Edn3* is expressed by stromal cells, which may include vascular smooth muscle cells.[52] *Ntf3* is expressed by nephron progenitors and developing nephrons, whereas *Artn1* does not appear to be expressed,[52] although their production by the vasculature at earlier stages is unknown.

Once established, continued axonal growth and survival relies on neurotrophic factors such as nerve growth factor (NGF). During nephrogenesis, NGF is produced by cortical, medullary, and ureteric stroma.[52,57] Additionally, it has been established that NGF is required for the complete sympathetic innervation of the kidney via its interaction with its innate receptor tropomyosin receptor kinase A.[57] Moreover, proper innervation also requires chemotactic guidance cues released by adjacent cells within the tissue. We and others have established that, in the kidneys, proper patterning of the neurovascular network is mediated by the guidance cue netrin-1.[30,40] However, the endothelium is the primary responder to netrin-1 guidance cues, with the nerves following the vascular pattern, suggesting that the vascular mural cells themselves play a significant role in guiding kidney innervation.[30] While it has been established that netrin-1 plays a key role in synapse formation and arterial innervation, we do not know whether the same is true in the kidneys.[58,59] Additional

studies are necessary to establish the full complement of cues necessary for proper kidney innervation and the establishment of functional crosstalk.

The diversity of kidney nerves

During kidney development, we found that both sensory and sympathetic nerves innervate the tissue early in development and branch following the arterial tree. Sensory nerves were classified as nociceptive by TRPV1$^+$ lineage tracing. The limitation of this approach is that, as neurons mature, they may not remain TRPV1$^+$. Therefore, and with our inability to identify a TRPV1 antibody that worked for immunolabeling, this lineage trace only serves as a proxy for TRPV1$^+$ nerves that innervate the kidneys from the onset. However, we were able to further classify the sensory neurons by their production of the neuropeptides CGRP and substance P. CGRP$^+$ nerves were identified earlier in development than substance P$^+$ nerves (E15.5 vs. E18.5), but both did not appear until innervation had already been established for several days. With the importance of neurotrophic factors for proper sensory afferent nerve function, these delays in production could be due to changes in molecular cues required for their specific growth and function.[60,61] The expression of their innate target receptor on kidney cells could also play an important role in triggering neuropeptide production. Despite these differences, all sensory nerve markers we investigated showed similar tracking with the vasculature and association with glomeruli and tubules around E18.5 to P0.

Recent studies have established that kidney stromal progenitors, juxtaglomerular cells, and glomerular mesangial cells express the mechanosensor *Piezo2*.[62,63] While our antibody labeling did not detect these PIEZO2$^+$ cells, this was also noted in the study by Mochida et al. where RNAScope *in situ* hybridization was necessary to detect *Piezo2* expression.[62] We identified PIEZO2$^+$ nerves in both mouse and human kidneys, where they associate with the vasculature, glomeruli, and tubules. We hypothesize that PIEZO2$^+$ fibers are poised to sense changes in pressure or volume within the kidneys. In the bladder, PIEZO2$^+$ urothelial cells communicate with pressure-sensitive PIEZO2$^+$ afferent nerves to mediate micturition.[22] However, further investigation is required to understand whether such communication between PIEZO2$^+$ kidney cells and PIEZO2$^+$ sensory neurons plays a role in development or physiological function. Interestingly, we found that axons loop in a hairpin fashion around glomeruli and tubules. Such anatomic positioning may enable the ability to sense changes in pressure, volume, filtration rate, and tubule physiology, ensuring homeostatic control. The looping may also enable signaling to multiple nephrons through varicosities or boutons that occur along the length of the axon.[3,19] These findings further emphasize the need for studies investigating the physiological role of sensory afferent nerves in the control of kidney development and function in health and disease.

In addition to sensory nerves, we showed that TH$^+$ sympathetic nerves innervate the developing kidney. TH$^+$ axons were detected as early as E14.5, and as development progressed, TH$^+$ fibers associated with the vasculature, tubules, and glomeruli. Association with these structures correlates with the known physiological functions of sympathetic nerves in modulating vascular tone, tubular sodium reabsorption, and renin release by juxtaglomerular cells.[3,26] Renal sympathetic nerve overactivity contributes to the

pathogenesis of hypertension. Thus, catheter-based renal denervation is an attractive therapeutic option to reduce blood pressure in hypertensive patients.[24,25,64] However, this procedure non-selectively targets all renal nerves, and with the significant overlap of sensory and sympathetic fibers innervating vasculature and glomeruli, a deeper understanding of the interplay between sympathetic and sensory nerves in the mediation of physiology may inform efforts to optimize ablation strategies.

Most visceral organs are innervated by both sympathetic and parasympathetic nerves. The kidney has been suggested to harbor parasympathetic nerves that enter along the renal vasculature.[65,66] Yet, there remains no significant anatomic evidence of extensive kidney parasympathetic innervation, and this remains a topic of debate. In our study, we observed TUBB3$^+$ nerve fibers colocalizing with the cholinergic marker VAChT; however, this could represent a subset of immature sympathetic nerves expressing VAChT. On the other hand, as development progressed and in adults, we observed VAChT$^+$ fibers associating with glomeruli which are more likely to represent mature, functional parasympathetic nerves. Additionally, the VAChT$^+$ fibers, albeit sparse, did not directly overlap with the NPY$^+$ signal. Cheng et al. have shown the presence of periarterial cholinergic nerves that were separate from sympathetic and sensory nerve fibers.[23] Together, these findings highlight the significant potential for parasympathetic activity in modulating kidney function, although further characterization and physiological validation are necessary.

Common DRG projections to organs of the urogenital system

The regulation of kidney homeostasis is in part maintained by neuronal modulation. Accurate mapping and knowing the molecular identity of all kidney nerves are necessary for understanding both their normal function and pathophysiological roles. However, studies have largely focused on renal sympathetic nerves, and only recently has the contribution of sensory neurons to physiological regulation been investigated more thoroughly.[3,15,67] Building on these previous studies, we found that kidney sensory innervation is substantial and molecularly diverse. Validation of sensory innervation was provided by retrograde tracing and identified the DRG origins of these nerves. While injections were restricted to the cortex, we cannot absolutely rule out minor leakage of the tracer into the pelvis and ureter, thus expanding the labeling to lower lumbar and sacral DRG, albeit at weaker levels. The majority of axons innervating the kidney project from T10–T13 and L1–L2. PIEZO2$^+$ neurons also traced to the DRG at these levels. FastBlue tracing performed in the mouse bladder and prostate revealed similar projection of neurons from T13, L1, L2, L6, and S1.[68] This suggests that organs of the genitourinary system may be innervated from common DRG.

Interestingly, CTB tracing also showed that contralateral DRG at L1 and L2 were labeled. These data suggest that some axons innervating the kidney might originate from contralateral DRG or that the DRG neurons send axons to both kidneys. Concurrent retrograde labeling of sensory nerves in the bladder and colon showed that dichotomizing afferent nerves coming from an individual DRG neuron innervate both the colon and the bladder.[69] Such connectivity is important for integrating sensory input from multiple organs and likely plays a major role in conditions such as pelvic pain disorders. DRG innervating

both kidneys or innervation from both contralateral and ipsilateral DRG would potentially enable greater coordination between the two kidneys.

Establishing crosstalk during kidney development

During development, nerves lie in close association with the vasculature, tubules, and glomeruli, suggesting potential functional crosstalk. Sympathetic and sensory nerves branch with the vasculature and dissociate to navigate through the tissue, where they loop around glomeruli and lie adjacent to tubules. Such close association and organization likely allow for the formation of neuroeffector junctions and the innervation of multiple structures. These fiber varicosities could impact adjacent kidney cells by establishing neuroeffector junctions more than 50 μm away from the neurotransmitter release site, allowing for diffusion throughout the interstitium and signaling to target cells.[3,8,70]

To investigate the potential for active signaling in the developing kidney, we assessed the localization of synapsin I, a major component of pre-synaptic vesicles and critical factor for axonogenesis.[71] We observed that synapsin I mainly localized near vasculature early in development, with the latter localization expanded to glomeruli and tubules. Such findings agree with our current understanding of kidney development and physiology. Mouse kidney development continues postnatally, contrary to human kidney development, which is finished before birth.[2] The mouse forms the majority of its nephrons toward the end of ureteric branching, with 40% of them differentiating after birth.[72] Yet, kidney function must be established very early on in newborn pups. Thus, it is likely important to establish proper innervation of the developing kidneys to regulate homeostasis. Whether kidney innervation also actively directs proper development as in other tissues, including the pancreas, salivary gland, and heart, remains unknown.[73-76]

Previously published scRNA-seq data from E18.5 kidneys[52] provide evidence that cells within the developing kidneys express a variety of receptors and postsynaptic markers, suggesting that they are competent to receive and respond to neuron-derived signals. Interestingly, several glutamate receptor subunits (*Gria1*, *Gria3*, *Gria4*, and *Grin3a*) are expressed by stromal or proximal tubule cells. While it has been established that glutamatergic signaling preserves the epithelial phenotype of proximal tubule cells through calcium signaling in the HK-2 cell line,[77] it remains unclear what role glutamate transport may play in the proper development of proximal tubules. Overall, the expression of neurotransmitter receptors and postsynaptic markers in the developing kidneys suggests the potential for several neuronal signaling mechanisms that regulate development and function.

Limitations of the study

Here, we detailed the spatial and temporal innervation of the kidneys. However, it is important to note some assumptions that guided our study. For the classification of noradrenergic sympathetic nerves, we used TH. However, some TH^+ axons in the developing kidneys may project from the DRG. Thus, we cannot omit that a certain percentage of these nerves may be sensory, although this is likely to be minor as embryonic TH production by sensory ganglia is minimal[51] and we observed only a small number of TH^+ somata within adult DRG. Additionally, the strong colocalization of TH and NPY in

adults suggests that sensory nerve production of TH is likely minor. We also utilized genetic lineage tracing to label sensory axons innervating the kidneys, with the assumption that most are TRPV1$^+$. However, lineage tracing does not accurately reflect changes in neuronal identity and may not encompass all sensory innervation. To comprehensively understand the full molecular profile of neurons innervating the kidneys, scRNA-seq of somata from sensory and sympathetic ganglia would be necessary. While scRNA-seq of the developing kidneys and SYN1$^+$ fibers near nephron structures suggests possible crosstalk, it does not validate active signaling. Higher-resolution electron microscopy and physiological assays would be necessary to decipher the nature of axon-kidney signaling junctions and when they become functional. Differences may also exist between human and mouse, and interrogating human scRNA-seq data may uncover species-specific mechanisms of crosstalk. Finally, we relied on the careful study of technical and biological replicates but did not quantify axon metrics aside from our adult glomerular quantitation. Hence, subtle differences among stages, classes of nerves, and sex may have been missed. Future investigations are necessary to parse out these details and to determine the significance of these nerves to overall kidney development.

STAR★METHODS

EXPERIMENTAL MODEL AND STUDY PARTICIPANT DETAILS

Mouse strains—All procedures and experiments were performed according to the guidelines of the National Institutes of Health Guide for the Care and Use of Laboratory Animals and were approved by the Institutional Animal Care and Use Committees of The University of North Carolina at Chapel Hill (protocols 19–183 and 22–136) and performed under the policies and recommendations of the International Association for the Study of Pain and approved by the Scripps Research Animal Care and Use Committee (protocol 08–0136). Mice were kept in standard housing with a 12-h light-dark cycle, with the room temperature kept around 22°C, and humidity between 30% and 80% (not controlled). Mice were kept on pelleted paper (Scripps) or corncob (UNC) bedding and provided with paper square nestlets and polyvinyl chloride pipe (Scripps) or hut (UNC) enrichment with *ad libitum* access to food and water. Adult Swiss Webster (Taconic stock #: SW MPF) and C57BL/6J (Jackson Labs (JAX) stock #: 000664) mice were purchased from the respective vendor for experiments and in house matings. Swiss Webster incrosses were utilized for all experiments involving embryonic and postnatal wild type mice. C57BL/6J mice were utilized for breeding of transgenic and knock-in lines and adult analyses. Mice utilized for adult analyses were 8 weeks to 4 months of age. *Trpv1*^{Cre} (JAX stock #: 017769)[78] were maintained as a homozygous line, Pod-Cre^{tg} mice (JAX stock #: 008205)[79] were maintained as heterozygotes, *R26*^{tdTomato} (JAX stock #: 007914)[80] mice were maintained as a homozygous line, and *Piezo2*$^{EGFP\text{-}IRES\text{-}Cre}$ (JAX stock #: 027719)[81] mice were maintained as heterozygotes. For genotyping, tail or ear clips were taken and incubated with DirectPCR lysis buffer (Viagen Biotech, 102-T) containing 10 μg/mL proteinase K (Sigma, 3115836001), incubated at 55°C overnight, and denatured at 95°C for 20 min the next day. Genotyping was performed using JAX genotyping protocols and recommended primers (see Table S1 for primer sequences) with the following PCR parameters: annealing temperature T = 58°C, elongation time T = 40 s, 35 cycles.

Human kidney tissue—Human kidney tissue samples ($n = 2$) were directly donated and de-identified samples obtained from the UNC Tissue Procurement Facility; all tissue is exempt from UNC IRB approval. Kidney tissue was flash-frozen in liquid nitrogen upon dissection without any fixation and stored at −80°C.

METHOD DETAILS

Tissue collection and processing—For all mouse experiments, matings were set up in the afternoon and copulation plugs found the following day were designated as embryonic day E0.5. The day of birth was considered postnatal day P0. This occurred at E19.5, births earlier or later than E19.5 were not utilized in these studies. At the desired developmental or adult time point, animals were sacrificed by CO_2 inhalation and death assured by cervical dislocation. Kidneys or whole urogenital systems were dissected in ice-cold 1x phosphate-buffered saline (PBS). Tail clips were utilized for genotyping as needed. To ensure biological significance, we analyzed a minimum of 3 animals per neuronal marker for both sexes at the following stages unless otherwise noted in the figure legend: E12.5, E13.5, E14.5, E15.5, E16.5, E18.5, P0, P1, P7, and adults. For tissue processing, all steps were performed on rotating shakers. Harvested kidneys or urogenital systems from embryonic and postnatal mice were fixed by immersion in fresh ice-cold 4% paraformaldehyde (PFA) (Electron Microscopy Sciences, 15714) in PBS at 4°C for 30 min, while kidneys obtained from adult mice were fixed by immersion in fresh ice-cold 4% PFA in PBS at 4°C for 2 h (except for NFH, NPY/TH, and CGRP/TH immunofluorescence; tissue processing is described below). Next, all kidneys were washed in ice-cold 1x PBS three times for 10 min each at room temperature and stored at 4°C in 1x PBS until use. All kidneys destined to be sectioned were incubated in 30% sucrose-PBS solution at 4°C overnight. The next day, kidneys were then embedded in Tissue-Plus O.C.T. Compound (Fisher Scientific, 23-730-571) and sectioned at 12 μm on a Leica cryostat CM1850. Slides were stored at −80°C until use.

Human kidney tissue was obtained as a frozen block. A small piece of tissue was removed with a razor blade, fixed for 10 min in 4% ice-cold PFA-PBS, and subsequent processing for cryosectioning and immunofluorescence was carried out as for the mouse.

Cholera toxin B (CTB) and AAV-PHP.S:FLEX-tdTomato retrograde tracing—Surgeries were performed similarly as previously described[82] with modifications. Briefly, mice were anesthetized with isoflurane inhalation and surgery started after all paw reflexes disappeared. The right kidney was accessed via flank incision after the animal was shaved from shoulder to rump and flank to spine with a shaver designed for pet grooming. After appropriate cleaning of the surgical site, the skin was pinched with tweezers and a cut of approximately 1cm from the spine and below the ribcage was made with scissors. A similar cut was made on the muscle layer underneath the skin, the kidney was exposed and carefully isolated with cotton-tip applicators from peripheral fat or connective tissues in order to not disrupt nerve connections. Tracers were slowly injected and the needle was left inside the tissue after injection for an additional 1 min to avoid back-leak. All injections were administered directly into kidney cortex through the renal capsule. For retrograde labeling of the DRG innervating the kidney, 4 injections of 3 μL 0.2% CTB-555 (Invitrogen, C34776)

were administered to 4 males and 4 females on a C57BL/6J or Swiss Webster background. For retrograde labeling of the PIEZO2^{+} nerves innervating the kidney, 4 injections of 5 μL of AAV-PHP.S particles that were produced from pAAV-FLEX-tdTomato were administered to 2 males and 2 females which were *Piezo2*$^{EGFP\text{-}IRES\text{-}Cre/+}$. pAAV-FLEX-tdTomato was a gift from Edward Boyden (Addgene viral prep #28306-PHP.S; http://n2t.net/addgene:28306; RRID:Addgene_28306; AAV-PHP.S courtesy of Viviana Gradinaru[43]). After injections, the muscle and skin were closed with sutures, and bupivacaine was administered for analgesia. After suturing, mice were housed in a clean cage with heat pads underneath until ambulatory. Mice were euthanized 4 days after CTB injections and 4 weeks after AAV-PHP.S injections. Mice were perfused with 30mL 1x PBS and 20mL 4% PFA in PBS with kidneys and DRG collected for tissue sectioning and imaging.

Immunofluorescence on tissue sections—Kidney sections for immunofluorescence were removed from the −80°C freezer and allowed to equilibrate to room temperature for 10 min. Sections were rehydrated, and the freezing medium was removed by incubating the slide in 1x PBS for 10 min in a Coplin jar. After rehydration, excess PBS was removed from the slide then a hydrophobic barrier was drawn around the section using a hydrophobic pap pen (Vector Laboratories, H-4000). Sections were incubated for 30 min in blocking solution (ice-cold PBS solution with 4% donkey serum (Equitech-Bio, SD30-0100), 1% bovine serum albumin (Fisher Scientific, BP9706-100), and 0.25% Triton X-100 (Fisher Scientific, BP151-500). Slides were then incubated at room temperature for 2 h covered from light with primary antibodies in block solution (see key resources table for antibodies and concentrations utilized; PIEZO2 antibodies were combined as a mixture for optimal detection although each worked independently as validated by co-immunostaining with GFP on DRG isolated from *Piezo2*$^{EGFP\text{-}IRES\text{-}Cre/+}$ mice). After primary incubation, slides were washed 3 times for 5 min at room temperature covered from light with wash solution (PBS +0.25% Triton X-100) before incubating them for 45 min at room temperature covered from light with the target appropriate Alexa Fluor secondary antibody (Life Technologies, 488, 568, or 647 conjugated; 1:1000) in blocking solution. Finally, slides were washed 4 times for 5 min at room temperature covered from light using wash solution with the last wash containing DAPI diluted at 1:10,000. Slides were mounted using ProLong Gold mounting media (Thermo Fisher Scientific, P36930) or VectaShield (Vector Laboratories (H-1000-10), sealed with No. 1.5 coverslips, and stored at room temp.

For the NFH, NPY/TH, and CGRP/TH immunofluorescence, C57BL/6J adult mice were euthanized via isoflurane overdose and transcardially perfused with 20 mL ice-cold PBS pH 7.4 followed by 30 mL ice-cold 4% PFA in PBS. Kidneys were dissected and fixed overnight in 4% PFA at 4°C. Kidneys were then rinsed in PBS and cryoprotected in 30% sucrose for 24–48 h at 4°C prior to embedding and freezing in Tissue-Tek O.C.T. Compound (Sakura, 4583). 20 μm sections were prepared on glass slides using a cryostat. Tissues were allowed to air-dry for 30 min at room temperature and hydrophobic barriers were drawn using a PAP pen. Slides were washed in PBS and blocked in 5% Normal Donkey Serum (for NPY immunofluorescence, Sigma-Aldrich, D9663) or Normal Goat Serum (Life Technologies, PCN5000) in PBS with 0.3% Triton X-100 (PBST) for 2 h at room temperature in a humidified chamber. Slides were incubated overnight at 4°C in the

following primary antibodies in 0.1% PBST: CGRP (Immunostar), TH (Abcam), NFH, or NPY (see key resources table for antibody details). Slides were washed in 0.3% PBST followed by PBS and then incubated for 2 h at room temperature in the following secondary antibodies in 0.1% PBST: donkey anti-goat 647 (Life Technologies, A21447, 1:1000), donkey anti-chicken 488 (Life Technologies, A78948, 1:1000), goat anti-Rabbit 647 (Life Technologies, A21245, 1:1000), goat anti-chicken 488 (Life Technologies, A11039,1:1000). Donkey secondary antibodies were used for NPY staining experiments and goat secondary antibodies were used for all other experiments. Samples were mounted using Fluoromount G Mounting Medium with DAPI (Thermo Fisher Scientific, 00-4959-52) and sealed with No. 1.5 coverslips and clear nail polish and stored at 4°C.

Whole-mount immunofluorescence and tissue clearing—For mouse embryonic and postnatal kidneys or urogenital systems (E12.5-P7), we used a modified version of the original iDISCO protocol (Renier et al., 2014) for whole-mount immunolabelling using validated antibodies and concentrations indicated in the key resources table. All steps are performed on rotating shakers. We first incubated whole pre-fixed tissue in 1mL blocking solution (ice-cold PBS solution with 10% (v/v) Heat Inactivated Sheep Serum (HISS) (Thermo Fisher Scientific, 16070096) and 0.5% (v/v) Triton X-100) for 1 h at room temperature. Then, we incubated the tissue in 1mL primary antibody in block solution for 7 days at 4°C while protected from light. The labeled tissue was then washed using 1mL wash buffer (PBS +0.25% Triton X-100) for a whole day at room temperature covered from light with wash solution changed every 1 h. After washing, labeled kidneys were incubated in 1mL secondary antibody (target appropriate Alexa Fluor 488, 568, or 647; Life Technologies) diluted in block solution at a concentration of 1:1000 for 3.5 days at 4°C while protected from light. After secondary antibody labeling, kidneys were washed again using 1mL wash buffer for a whole day at room temperature covered from light with wash solution changed every 1 h. Before optical clearing, successful labeling was checked on a widefield Leica fluorescent microscope (Leica DMi8). Labeled kidneys were then embedded in 1% agarose (Fisher Scientific, BP160-500) gel made with 1x TAE (tris-acetate-EDTA), the agarose block was cut to a size of 5 mm × 5 mm to ensure proper mounting on the light-sheet microscope. All clearing steps were carried out with samples protected from light. To clear kidneys, we first dehydrated the agarose block in a methanol-H_20 (Fisher Scientific, A433P-4) series wash at room temperature (25%, 50%, 75%, and 100%) for 1 h each minimum. Next, dehydrated agarose blocks were incubated in 66% v/v dichloromethane (DCM) (Sigma, 270997)/33% v/v methanol for 3 h at room temperature. Following this, the agarose blocks were then incubated in 100% DCM for 15min x 2 at room temperature. Finally, the fully dehydrated agarose blocks were incubated in 100% v/v dibenzyl ether (DBE) (Sigma, 33630) at room temperature. The blocks became transparent and invisible within 5-7hr and were stored in DBE until imaging. The DBE was changed out for fresh DBE before imaging the sample.

For human kidney tissue whole-mount, a piece of frozen tissue was removed with a razor blade, fixed for 30 min in 4% ice-cold PFA in PBS at 4°C, and subsequently washed three times in PBS with 2.5Units/mL of Heparin (Sigma, H4784) at room temperature for 30min each. Samples were then washed three times in PBS with 2.5Units/mL Heparin and

1% CHAPS (Sigma, C3023) at room temperature for 30min each. Human tissue was then blocked in 2-3mL block solution (PBS with 10% (v/v) HISS, 2.5Units/mL Heparin, and 1% CHAPS) for 1 h at 4°C. All subsequent steps were carried out with samples protected from light. Tissues were incubated in 2-3mL primary antibody (see key resources table) diluted in block solution for 7 days at 4°C. The labeled tissue was then washed using wash buffer (PBS solution with 1% v/v CHAPS) for a whole day at room temperature with wash solution changed every 1 h. After washing, labeled kidneys were incubated in 1mL secondary antibody (target appropriate Alexa Fluor 488, 568, or 647; Life Technologies) diluted in block solution at a concentration of 1:1000 for 3 days at 4°C. After secondary antibody labeling, kidneys were washed again using wash buffer for a whole day at room temperature with wash solution changed every 1 h. Clearing was conducted as described for mouse tissues.

3D light-sheet and confocal imaging—All whole-mount images were obtained using the LaVision BioTec UltraMicroscope II (UM II, Miltenyi Biotec) and the UltraMicroscope Blaze (Blaze, Miltenyi Biotec) light-sheet system at the UNC Microscopy Services Laboratory (MSL). The UM II light-sheet is outfitted with an Andor Zyla 5.5 sCMOS detector, an Olympus MVPLAPO 2X/0.5 objective coupled to a zoom body ranging from 1.26x to 12.6x with a corrected dipping cap and a working distance of 5.7mm. Imaging was conducted in 100% DBE. The Blaze light-sheet is outfitted with a 4.2 Megapixel sCMOS camera, an MI Plan 4x/0.35 objective coupled to a total zoom ranging from 2.4x to 10x with a corrected dipping cap and a working distance of ≤ 16mm. Imaging was conducted in MACS Imaging Solution (Miltenyi Biotec, 130-128-511). All wholemount images in this study were imaged with laser wavelengths: 488, 561, and 647nm as well as 3 angled light-sheet with specific parameters. All tiff images are generated in 16-bit. See Table S2 for specific imaging parameters.

Confocal images were primarily obtained using either Zeiss 880 confocal laser scanning microscope in the UNC Hooker Imaging Core (HIC) or the Zeiss 900 confocal laser scanning microscope in the UNC MSL. The Zeiss 880 uses the Zen 2 software with 34-channel gallium arsenide phosphide (GaAsP) detectors. All images obtained were imaged using a Plan-Neofluar 40x/NA:1.3 oil objective or Plan-Apo 20x/NA:0.8 with the following working distance respectively: 0.21mm and 0.55mm. The Zeiss 900 uses the Zen blue software with three gallium arsenide phosphide PMT (GaAsP) detectors. All images obtained were imaged using a Plan-Apo 40x/NA:1.4 oil objective with the working distance of 0.21mm. Pinhole size of 1AU set on the longest wavelength fluorophore with the same diameter size for all the rest. An Andor Dragonfly Spinning Disk Confocal (MSL), Zeiss confocal LSM 780, Nikon AX confocal, Evident Sci VS200 Slide Scanning System (HIC), and Leica DMi8 Inverted Fluorescent Widefield Microscope were also utilized as indicated in Table S2 where all image acquisition settings can be found.

Image processing—Images, 3D volume, and movies were generated using Imaris × 64 software version 9.9.1. All stack images obtained from light-sheet imaging were first converted into an imaris file (.ims) using Imaris File Converter version 9.8.2. All wholemount images and videos were obtained using the "snapshot" and "animation" tools

in Imaris 9.9.1. Files obtained with confocal microscopes were converted into an Imaris file using Imaris File Converter 9.8.2. Tilescan images were stitched with 20% overlapped using Imaris stitcher 9.9.1 and image analysis was done in Imaris version 9.9.1.

QUANTIFICATION AND STATISTICAL ANALYSIS

CGRP/TH glomeruli quantification—Maximum intensity z-projections were generated and glomeruli were identified from the DAPI signal as regions of interest (ROIs). Each individual ROI was manually assessed for the presence of TH or CGRP immunoreactivity at the Bowman's capsule or at the juxtaglomerular region adjoining the glomerulus and the arterioles. ROI with immunoreactivity at either location were determined to be innervated. For the TH staining, substantial non-neuronal tubular immunoreactivity was observed that was readily distinguishable from nerve fibers. The tubular immunoreactivity was not used to quantify innervation. Fiji (2.0.0) and Prism (10.1.1) software were utilized for analyses.

Receptor and postsynaptic marker scRNA-seq enrichment—To identify the kidney cell populations in which nerve associated receptors and markers were expressed, the selected genes were analyzed for their relative enrichment within the scRNA-seq data from E18.5 kidneys.[52] Heatmaps were generated in R (https://www.r-project.org/) using the ggplot2 package[83] and ComplexHeatmap.[84] Log fold change values were obtained from Combes et al., 2019 Table S1 "lookup" tab.[52]

Supplementary Material

Refer to Web version on PubMed Central for supplementary material.

ACKNOWLEDGMENTS

We thank members of the O'Brien Lab for their critical insights throughout the project. We would like to thank Dr. Pablo Ariel, Director of the UNC Microscopy Services Laboratory (MSL), for expert training in light-sheet image acquisition and analysis and lending his expertise throughout the project. We thank Dr. Wendy Salmon, Director of the UNC Hooker Imaging Core (HIC), for confocal microscopy imaging training. The MSL and HIC are supported by the NIH P30CA016086 Cancer Center Core Support Grant to the UNC Lineberger Comprehensive Cancer Center. Light-sheet microscopy at MSL is supported in part by the North Carolina Biotech Center Institutional Support Grant 2016-IDG-1016, and the Andor Dragonfly microscope was funded with support from NIH grant S10OD030223. This work was supported by AHA Predoctoral Fellowship 24PRE1241584 (to P.-E.Y.N.), NIH TRIO NRSA Training Grant TL1DK139567 (to S.R.M.), NIH R01DK121014 (to L.L.O.), NIH R01DA044481 and Department of Defense Neurosensory Research Award W81XWH-15-1-0076 (to G.S.), the New York Stem Cell Foundation (to G.S.), NIH K99NS133478 (to R.Z.H.), and a Helen Lyng White postdoctoral fellowship (to A.T.).

REFERENCES

1. May CN, Frithiof R, Hood SG, McAllen RM, McKinley MJ, and Ramchandra R (2010). Specific control of sympathetic nerve activity to the mammalian heart and kidney. Exp. Physiol 95, 34–40. 10.1113/expphysiol.2008.046342. [PubMed: 19617268]
2. McMahon AP (2016). Development of the Mammalian Kidney. Curr. Top. Dev. Biol 117, 31–64. 10.1016/bs.ctdb.2015.10.010. [PubMed: 26969971]
3. Osborn JW, Tyshynsky R, and Vulchanova L (2021). Function of Renal Nerves in Kidney Physiology and Pathophysiology. Annu. Rev. Physiol 83, 429–450. 10.1146/annurev-physiol-031620-091656. [PubMed: 33566672]
4. Booth LC, May CN, and Yao ST (2015). The role of the renal afferent and efferent nerve fibers in heart failure. Front. Physiol 6, 270. 10.3389/fphys.2015.00270. [PubMed: 26483699]

5. Knuepfer MM, and Schramm LP (1987). The conduction velocities and spinal projections of single renal afferent fibers in the rat. Brain Res. 435, 167–173. 10.1016/0006-8993(87)91598-8. [PubMed: 3427451]
6. Simon OR, and Schramm LP (1983). Spinal superfusion of dopamine excites renal sympathetic nerve activity. Neuropharmacology 22, 287–293. 10.1016/0028-3908(83)90242-3. [PubMed: 6843790]
7. Stella A, and Zanchetti A (1991). Functional role of renal afferents. Physiol. Rev 71, 659–682. 10.1152/physrev.1991.71.3.659. [PubMed: 1647536]
8. DiBona GF, and Kopp UC (1997). Neural control of renal function. Physiol. Rev 77, 75–197. 10.1152/physrev.1997.77.1.75. [PubMed: 9016301]
9. Malpas SC (2010). Sympathetic Nervous System Overactivity and Its Role in the Development of Cardiovascular Disease. Physiol. Rev 90, 513–557. 10.1152/physrev.00007.2009. [PubMed: 20393193]
10. Sata Y, Head GA, Denton K, May CN, and Schlaich MP (2018). Role of the Sympathetic Nervous System and Its Modulation in Renal Hypertension. Front. Med 5, 82. 10.3389/fmed.2018.00082.
11. Bhatt DL, Vaduganathan M, Kandzari DE, Leon MB, Rocha-Singh K, Townsend RR, Katzen BT, Oparil S, Brar S, DeBruin V, et al. (2022). Long-term outcomes after catheter-based renal artery denervation for resistant hypertension: final follow-up of the randomised SYMPLICITY HTN-3 Trial. Lancet 400, 1405–1416. 10.1016/S0140-6736(22)01787-1. [PubMed: 36130612]
12. Denton KM, Luff SE, Shweta A, and Anderson WP (2004). DIFFERENTIAL NEURAL CONTROL OF GLOMERULAR ULTRAFILTRATION. Clin. Exp. Pharmacol. Physiol 31, 380–386. 10.1111/j.1440-1681.2004.04002.x. [PubMed: 15191417]
13. DiBona GF (2000). Nervous Kidney. Hypertension 36, 1083–1088. 10.1161/01.hyp.36.6.1083. [PubMed: 11116129]
14. Fujisawa Y, Nagai Y, Lei B, Nakano D, Fukui T, Hitomi H, Mori H, Masaki T, and Nishiyama A (2011). Roles of central renin-angiotensin system and afferent renal nerve in the control of systemic hemodynamics in rats. Hypertens. Res 34, 1228–1232. 10.1038/hr.2011.115. [PubMed: 21796126]
15. Banek CT, Knuepfer MM, Foss JD, Fiege JK, Asirvatham-Jeyaraj N, Van Helden D, Shimizu Y, and Osborn JW (2016). Resting Afferent Renal Nerve Discharge and Renal Inflammation: Elucidating the Role of Afferent and Efferent Renal Nerves in Deoxycorticosterone Acetate Salt Hypertension. Hypertension 68, 1415–1423. 10.1161/HYPERTENSIONAHA.116.07850. [PubMed: 27698066]
16. Veelken R, Vogel E-M, Hilgers K, Amann K, Hartner A, Sass G, Neuhuber W, and Tiegs G (2008). Autonomic renal denervation ameliorates experimental glomerulonephritis. J. Am. Soc. Nephrol 19, 1371–1378. 10.1681/ASN.2007050552. [PubMed: 18400940]
17. Xiao L, Kirabo A, Wu J, Saleh MA, Zhu L, Wang F, Takahashi T, Loperena R, Foss JD, Mernaugh RL, et al. (2015). Renal Denervation Prevents Immune Cell Activation and Renal Inflammation in Angiotensin II-Induced Hypertension. Circ. Res 117, 547–557. 10.1161/CIRCRESAHA.115.306010. [PubMed: 26156232]
18. Kaur J, Young BE, and Fadel PJ (2017). Sympathetic Overactivity in Chronic Kidney Disease: Consequences and Mechanisms. Int. J. Mol. Sci 18, 1682. 10.3390/ijms18081682. [PubMed: 28767097]
19. Tyshynsky R, Sensarma S, Riedl M, Bukowy J, Schramm LP, Vulchanova L, and Osborn JW (2023). Periglomerular afferent innervation of the mouse renal cortex. Front. Neurosci 17, 974197. 10.3389/fnins.2023.974197. [PubMed: 36777644]
20. Kopp UC (2015). Role of renal sensory nerves in physiological and pathophysiological conditions. Am. J. Physiol. Regul. Integr. Comp. Physiol 308, R79–R95. 10.1152/ajpregu.00351.2014. [PubMed: 25411364]
21. Lam RM, von Buchholtz LJ, Falgairolle M, Osborne J, Frangos E, Servin-Vences MR, Nagel M, Nguyen MQ, Jayabalan M, Saade D, et al. (2023). PIEZO2 and perineal mechanosensation are essential for sexual function. Science 381, 906–910. 10.1126/science.adg0144. [PubMed: 37616369]

22. Marshall KL, Saade D, Ghitani N, Coombs AM, Szczot M, Keller J, Ogata T, Daou I, Stowers LT, Bönnemann CG, et al. (2020). PIEZO2 in sensory neurons and urothelial cells coordinates urination. Nature 588, 290–295. 10.1038/s41586-020-2830-7. [PubMed: 33057202]
23. Cheng X, Zhang Y, Chen R, Qian S, Lv H, Liu X, and Zeng S (2022). Anatomical Evidence for Parasympathetic Innervation of the Renal Vasculature and Pelvis. J. Am. Soc. Nephrol 33, 2194–2210. 10.1681/ASN.2021111518. [PubMed: 36253054]
24. Krum H, Schlaich M, and Sobotka P (2013). Renal sympathetic nerve ablation for treatment-resistant hypertension. Br. J. Clin. Pharmacol 76, 495–503. 10.1111/bcp.12171. [PubMed: 23819768]
25. Krum H, Schlaich MP, Sobotka PA, Böhm M, Mahfoud F, Rocha-Singh K, Katholi R, and Esler MD (2014). Percutaneous renal denervation in patients with treatment-resistant hypertension: final 3-year report of the Symplicity HTN-1 study. Lancet 383, 622–629. 10.1016/s0140-6736(13)62192-3. [PubMed: 24210779]
26. Osborn JW, and Foss JD (2017). Renal Nerves and Long-Term Control of Arterial Pressure. Compr. Physiol 7, 263–320. 10.1002/cphy.c150047. [PubMed: 28333375]
27. Schlaich MP, Sobotka PA, Krum H, Lambert E, and Esler MD (2009). Renal Sympathetic-Nerve Ablation for Uncontrolled Hypertension. N. Engl. J. Med 361, 932–934. 10.1056/nejmc0904179. [PubMed: 19710497]
28. Symplicity HTN-2 Investigators; Esler MD, Krum H, Sobotka PA, Schlaich MP, Schsmieder RE, and Böhm M (2010). Renal sympathetic denervation in patients with treatment-resistant hypertension (The Symplicity HTN-2 Trial): a randomised controlled trial. Lancet 376, 1903–1909. 10.1016/S0140-6736(10)62039-9. [PubMed: 21093036]
29. Townsend RR, Mahfoud F, Kandzari DE, Kario K, Pocock S, Weber MA, Ewen S, Tsioufis K, Tousoulis D, Sharp ASP, et al. (2017). Catheter-based renal denervation in patients with uncontrolled hypertension in the absence of antihypertensive medications (SPYRAL HTN-OFF MED): a randomised, sham-controlled, proof-of-concept trial. Lancet 390, 2160–2170. 10.1016/s0140-6736(17)32281-x. [PubMed: 28859944]
30. Honeycutt SE, N'Guetta P-EY, Hardesty DM, Xiong Y, Cooper SL, Stevenson MJ, and O'Brien LL (2023). Netrin-1 directs vascular patterning and maturity in the developing kidney. Development 150. 10.1242/dev.201886.
31. Tarnick J, Elhendawi M, Holland I, Chang Z, and Davies JA (2023). Innervation of the developing kidney in vivo and in vitro. Biol. Open 12, bio060001. 10.1242/bio.060001. [PubMed: 37439314]
32. Barajas L, Liu L, and Powers K (1992). Anatomy of the renal innervation: intrarenal aspects and ganglia of origin. Can. J. Physiol. Pharmacol 70, 735–749. 10.1139/y92-098. [PubMed: 1423018]
33. Bell C, and McLachlan EM (1982). Dopaminergic neurons in sympathetic ganglia of the dog. Proc. R. Soc. Lond. B Biol. Sci 215, 175–190. 10.1098/rspb.1982.0036. [PubMed: 6127703]
34. Ferguson M, Ryan GB, and Bell C (1986). Localization of sympathetic and sensory neurons innervating the rat kidney. J. Auton. Nerv. Syst 16, 279–288. 10.1016/0165-1838(86)90034-2. [PubMed: 2427560]
35. Ferguson M, Ryan GB, and Bell C (1988). The innervation of the renal cortex in the dog. Cell Tissue Res. 253, 539–546. 10.1007/bf00219744. [PubMed: 2902923]
36. Kuo DC, de Groat WC, and Nadelhaft I (1982). Origin of sympathetic efferent axons in the renal nerves of the cat. Neurosci. Lett 29, 213–218. 10.1016/0304-3940(82)90319-6. [PubMed: 6179014]
37. Donovan MK, Wyss JM, and Winternitz SR (1983). Localization of renal sensory neurons using the fluorescent dye technique. Brain Res. 259, 119–122. 10.1016/0006-8993(83)91072-7. [PubMed: 6824924]
38. Weiss ML, and Chowdhury SI (1998). The renal afferent pathways in the rat: a pseudorabies virus study. Brain Res. 812, 227–241. 10.1016/s0006-8993(98)00950-0. [PubMed: 9813344]
39. Daniel E, Azizoglu DB, Ryan AR, Walji TA, Chaney CP, Sutton GI, Carroll TJ, Marciano DK, and Cleaver O (2018). Spatiotemporal heterogeneity and patterning of developing renal blood vessels. Angiogenesis 21, 617–634. 10.1007/s10456-018-9612-y. [PubMed: 29627966]

40. Luo PM, Gu X, Chaney C, Carroll T, and Cleaver O (2023). Stromal netrin-1 coordinates renal arteriogenesis and mural cell differentiation. Development 150, dev201884. 10.1242/dev.201884. [PubMed: 37823339]
41. Stocker SD, and Sullivan JB (2023). Deletion of the Transient Receptor Potential Vanilloid 1 Channel Attenuates Sympathoexcitation and Hypertension and Improves Glomerular Filtration Rate in 2-Kidney-1-Clip Rats. Hypertension 80, 1671–1682. 10.1161/HYPERTENSIONAHA.123.21153. [PubMed: 37334698]
42. Coste B, Mathur J, Schmidt M, Earley TJ, Ranade S, Petrus MJ, Dubin AE, and Patapoutian A (2010). Piezo1 and Piezo2 are essential components of distinct mechanically activated cation channels. Science 330, 55–60. 10.1126/science.1193270. [PubMed: 20813920]
43. Chan KY, Jang MJ, Yoo BB, Greenbaum A, Ravi N, Wu W-L, Sánchez-Guardado L, Lois C, Mazmanian SK, Deverman BE, and Gradinaru V (2017). Engineered AAVs for efficient noninvasive gene delivery to the central and peripheral nervous systems. Nat. Neurosci 20, 1172–1179. 10.1038/nn.4593. [PubMed: 28671695]
44. Tiniakos D, Anagnostou V, Stavrakis S, Karandrea D, Agapitos E, and Kittas C (2004). Ontogeny of intrinsic innervation in the human kidney. Anat. Embryol 209, 41–47. 10.1007/s00429-004-0420-3.
45. Torres H, Huesing C, Burk DH, Molinas AJR, Neuhuber WL, Berthoud H-R, Münzberg H, Derbenev AV, and Zsombok A (2021). Sympathetic innervation of the mouse kidney and liver arising from prevertebral ganglia. Am. J. Physiol. Regul. Integr. Comp. Physiol 321, R328–R337. 10.1152/ajpregu.00079.2021. [PubMed: 34231420]
46. Meerschaert KA, Adelman PC, Friedman RL, Albers KM, Koerber HR, and Davis BM (2020). Unique Molecular Characteristics of Visceral Afferents Arising from Different Levels of the Neuraxis: Location of Afferent Somata Predicts Function and Stimulus Detection Modalities. J. Neurosci 40, 7216–7228. 10.1523/JNEUROSCI.1426-20.2020. [PubMed: 32817244]
47. Brumovsky PR, La JH, McCarthy CJ, Hökfelt T, and Gebhart GF (2012). Dorsal root ganglion neurons innervating pelvic organs in the mouse express tyrosine hydroxylase. Neuroscience 223, 77–91. 10.1016/j.neuroscience.2012.07.043. [PubMed: 22858598]
48. Howard MJ (2005). Mechanisms and perspectives on differentiation of autonomic neurons. Dev. Biol 277, 271–286. 10.1016/j.yd-bio.2004.09.034. [PubMed: 15617674]
49. Keast JR (1995). Visualization and immunohistochemical characterization of sympathetic and parasympathetic neurons in the male rat major pelvic ganglion. Neuroscience 66, 655–662. 10.1016/0306-4522(94)00595-v. [PubMed: 7644029]
50. Wanigasekara Y, Kepper ME, and Keast JR (2003). Immunohistochemical characterisation of pelvic autonomic ganglia in male mice. Cell Tissue Res. 311, 175–185. 10.1007/s00441-002-0673-1. [PubMed: 12596037]
51. Smith-Anttila CJA, Morrison V, and Keast JR (2021). Spatiotemporal mapping of sensory and motor innervation of the embryonic and postnatal mouse urinary bladder. Dev. Biol 476, 18–32. 10.1016/j.ydbio.2021.03.008. [PubMed: 33744254]
52. Combes AN, Phipson B, Lawlor KT, Dorison A, Patrick R, Zappia L, Harvey RP, Oshlack A, and Little MH (2019). Single cell analysis of the developing mouse kidney provides deeper insight into marker gene expression and ligand-receptor crosstalk. Development 146, dev178673. 10.1242/dev.178673. [PubMed: 31118232]
53. Little MH (2015). Improving our resolution of kidney morphogenesis across time and space. Curr. Opin. Genet. Dev 32, 135–143. 10.1016/j.gde.2015.03.001. [PubMed: 25819979]
54. Glebova NO, and Ginty DD (2005). GROWTH AND SURVIVAL SIGNALS CONTROLLING SYMPATHETIC NERVOUS SYSTEM DEVELOPMENT. Annu. Rev. Neurosci 28, 191–222. 10.1146/annurev.neuro.28.061604.135659. [PubMed: 16022594]
55. Kuruvilla R, Zweifel LS, Glebova NO, Lonze BE, Valdez G, Ye H, and Ginty DD (2004). A neurotrophin signaling cascade coordinates sympathetic neuron development through differential control of TrkA trafficking and retrograde signaling. Cell 118, 243–255. 10.1016/j.cell.2004.06.021. [PubMed: 15260993]

56. Makita T, Sucov HM, Gariepy CE, Yanagisawa M, and Ginty DD (2008). Endothelins are vascular-derived axonal guidance cues for developing sympathetic neurons. Nature 452, 759–763. 10.1038/nature06859. [PubMed: 18401410]
57. Glebova NO, and Ginty DD (2004). Heterogeneous requirement of NGF for sympathetic target innervation in vivo. J. Neurosci 24, 743–751. 10.1523/JNEUROSCI.4523-03.2004. [PubMed: 14736860]
58. Zheng M, Chen R, Chen H, Zhang Y, Chen J, Lin P, Lan Q, Yuan Q, Lai Y, Jiang X, et al. (2018). Netrin-1 Promotes Synaptic Formation and Axonal Regeneration via JNK1/c-Jun Pathway after the Middle Cerebral Artery Occlusion. Front. Cell. Neurosci 12, 13. 10.3389/fncel.2018.00013. [PubMed: 29487502]
59. Brunet I, Gordon E, Han J, Cristofaro B, Broqueres-You D, Liu C, Bouvrée K, Zhang J, del Toro R, Mathivet T, et al. (2014). Netrin-1 controls sympathetic arterial innervation. J. Clin. Invest 124, 3230–3240. 10.1172/JCI75181. [PubMed: 24937433]
60. Ernsberger U, Deller T, and Rohrer H (2020). The diversity of neuronal phenotypes in rodent and human autonomic ganglia. Cell Tissue Res. 382, 201–231. 10.1007/s00441-020-03279-6. [PubMed: 32930881]
61. Golden JP, Hoshi M, Nassar MA, Enomoto H, Wood JN, Milbrandt J, Gereau RW, Johnson EM Jr., and Jain S (2010). RET signaling is required for survival and normal function of nonpeptidergic nociceptors. J. Neurosci 30, 3983–3994. 10.1523/JNEUROSCI.5930-09.2010. [PubMed: 20237269]
62. Mochida Y, Ochiai K, Nagase T, Nonomura K, Akimoto Y, Fukuhara H, Sakai T, Matsumura G, Yamaguchi Y, and Nagase M (2022). Piezo2 expression and its alteration by mechanical forces in mouse mesangial cells and renin-producing cells. Sci. Rep 12, 4197. 10.1038/s41598-022-07987-7. [PubMed: 35273307]
63. Hill RZ, Shirvan S, Burquez S, Dubin AE, Servin-Vences MR, Miner JH, and Patapoutian A (2023). Renal mechanotransduction is an essential regulator of renin. bioRxiv. 10.1101/2023.11.04.565646.
64. Esler MD, Krum H, Schlaich M, Schmieder RE, Böhm M, and Sobotka PA; Symplicity HTN-2 Investigators (2012). Renal Sympathetic Denervation for Treatment of Drug-Resistant Hypertension. Circulation 126, 2976–2982. 10.1161/circulationaha.112.130880. [PubMed: 23248063]
65. Furness JB (1999). The Autonomic Nervous System and Its Effectors by Alison Brading. Trends Neurosci. 22, 568–569. 10.1016/s0166-2236(99)01485-x.
66. Mitchell GAG (1950). THE NERVE SUPPLY OF THE KIDNEYS. Acta Anat. 10, 1–37. 10.1159/000140455. [PubMed: 14777246]
67. Ong J, Kinsman BJ, Sved AF, Rush BM, Tan RJ, Carattino MD, and Stocker SD (2019). Renal sensory nerves increase sympathetic nerve activity and blood pressure in 2-kidney 1-clip hypertensive mice. J. Neurophysiol. 122, 358–367. 10.1152/jn.00173.2019. [PubMed: 31091159]
68. Lee S, Yang G, Xiang W, and Bushman W (2016). Retrograde double-labeling demonstrates convergent afferent innervation of the prostate and bladder. Prostate 76, 767–775. 10.1002/pros.23170. [PubMed: 26939943]
69. Christianson JA, Liang R, Ustinova EE, Davis BM, Fraser MO, and Pezzone MA (2007). Convergence of bladder and colon sensory innervation occurs at the primary afferent level. Pain 128, 235–243. 10.1016/j.pain.2006.09.023. [PubMed: 17070995]
70. Barajas L, Powers K, and Wang P (1984). Innervation of the renal cortical tubules: a quantitative study. Am. J. Physiol 247, F50–F60. 10.1152/ajprenal.1984.247.1.f50. [PubMed: 6742205]
71. Chin LS, Li L, Ferreira A, Kosik KS, and Greengard P (1995). Impairment of axonal development and of synaptogenesis in hippocampal neurons of synapsin I-deficient mice. Proc. Natl. Acad. Sci. USA 92, 9230–9234. [PubMed: 7568107]
72. Smyth IM (2021). Monkeying about with Nephron Formation. J. Am. Soc. Nephrol 32, 1011–1013. 10.1681/ASN.2021030320. [PubMed: 33827903]
73. Borden P, Houtz J, Leach SD, and Kuruvilla R (2013). Sympathetic innervation during development is necessary for pancreatic islet architecture and functional maturation. Cell Rep. 4, 287–301. 10.1016/j.celrep.2013.06.019. [PubMed: 23850289]

74. Re K, and Sj B (2015). Innervating sympathetic neurons regulate heart size and the timing of cardiomyocyte cell cycle withdrawal. J Physiol. 593, 5057–73. 10.1113/JP270917. [PubMed: 26420487]

75. Tampakakis E, Gangrade H, Glavaris S, Htet M, Murphy S, Lin BL, Liu T, Saberi A, Miyamoto M, Kowalski W, et al. (2021). Heart neurons use clock genes to control myocyte proliferation. Sci. Adv 7, eabh4181. 10.1126/sciadv.abh4181. [PubMed: 34851661]

76. Nedvetsky PI, Emmerson E, Finley JK, Ettinger A, Cruz-Pacheco N, Prochazka J, Haddox CL, Northrup E, Hodges C, Mostov KE, et al. (2014). Parasympathetic innervation regulates tubulogenesis in the developing salivary gland. Dev. Cell 30, 449–462. 10.1016/j.devcel.2014.06.012. [PubMed: 25158854]

77. Bozic M, de Rooij J, Parisi E, Ortega MR, Fernandez E, and Valdivielso JM (2011). Glutamatergic signaling maintains the epithelial phenotype of proximal tubular cells. J. Am. Soc. Nephrol 22, 1099–1111. 10.1681/ASN.2010070701. [PubMed: 21597037]

78. Cavanaugh DJ, Chesler AT, Jackson AC, Sigal YM, Yamanaka H, Grant R, O'Donnell D, Nicoll RA, Shah NM, Julius D, and Basbaum AI (2011). Trpv1 reporter mice reveal highly restricted brain distribution and functional expression in arteriolar smooth muscle cells. J. Neurosci 31, 5067–5077. 10.1523/JNEUROSCI.6451-10.2011. [PubMed: 21451044]

79. Moeller MJ, Sanden SK, Soofi A, Wiggins RC, and Holzman LB (2003). Podocyte-specific expression of cre recombinase in transgenic mice. Genesis 35, 39–42. 10.1002/gene.10164. [PubMed: 12481297]

80. Madisen L, Zwingman TA, Sunkin SM, Oh SW, Zariwala HA, Gu H, Ng LL, Palmiter RD, Hawrylycz MJ, Jones AR, et al. (2010). A robust and high-throughput Cre reporting and characterization system for the whole mouse brain. Nat. Neurosci 13, 133–140. 10.1038/nn.2467. [PubMed: 20023653]

81. Woo S-H, Ranade S, Weyer AD, Dubin AE, Baba Y, Qiu Z, Petrus M, Miyamoto T, Reddy K, Lumpkin EA, et al. (2014). Piezo2 is required for Merkel-cell mechanotransduction. Nature 509, 622–626. 10.1038/nature13251. [PubMed: 24717433]

82. Woodard LE, Welch RC, Williams FM, Luo W, Cheng J, and Wilson MH (2018). Hydrodynamic Renal Pelvis Injection for Non-viral Expression of Proteins in the Kidney. J. Vis. Exp 56324, 56324. 10.3791/56324.

83. Wickham H. (2009). ggplot2: Elegant Graphics for Data Analysis (Springer).

84. Gu Z, Eils R, and Schlesner M (2016). Complex heatmaps reveal patterns and correlations in multidimensional genomic data. Bioinformatics 32, 2847–2849. 10.1093/bioinformatics/btw313. [PubMed: 27207943]

Highlights

- Kidney innervation commences at E13.5 following renal arterial differentiation
- Sympathetic and sensory nerves innervate the kidney, extending to the cortex
- Nerves associate with glomeruli and tubules, similar to the adult human kidneys
- Retrograde tracing shows sensory afferents project from T10–L2 dorsal root ganglia

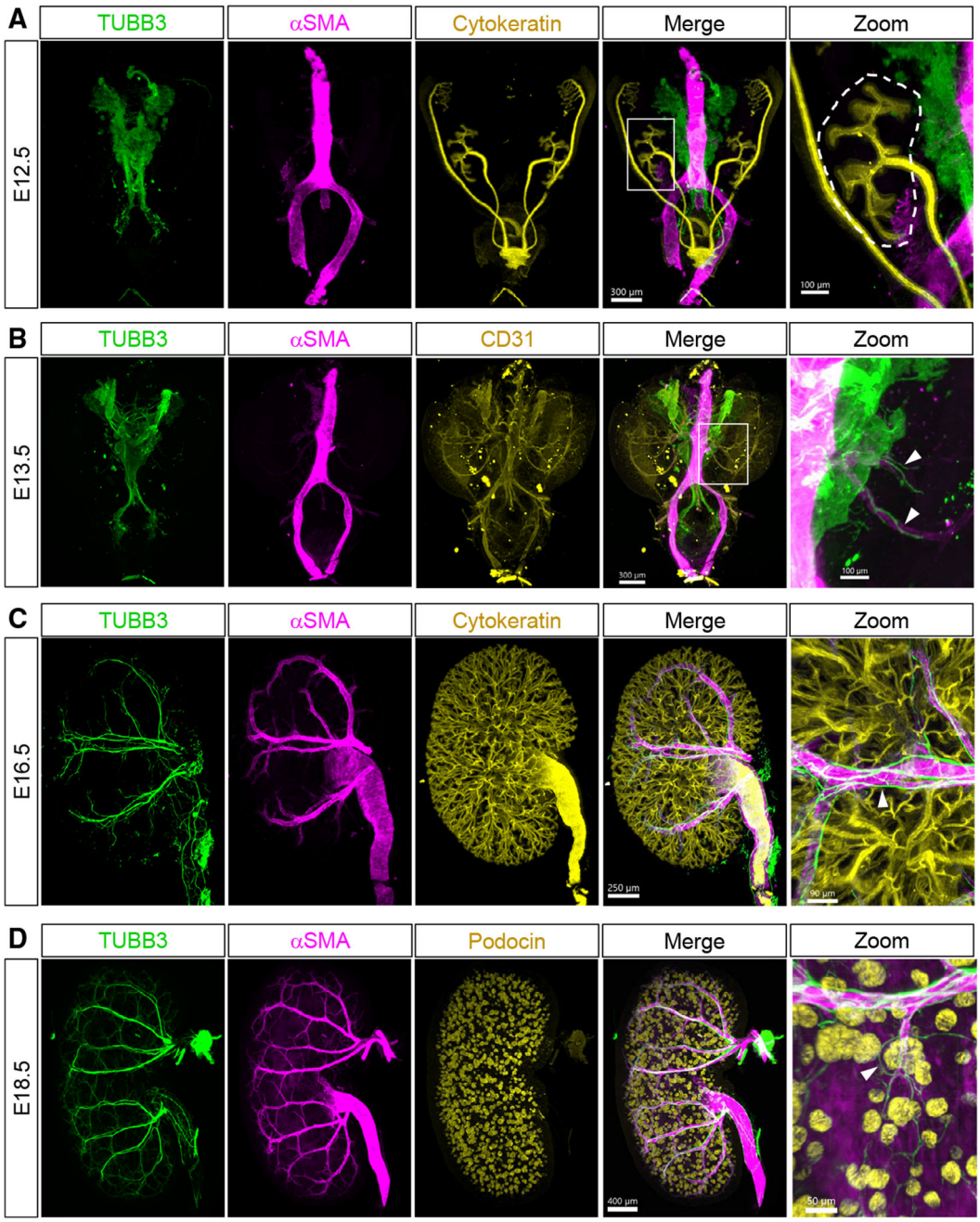

Figure 1. Kidney innervation commences at E13.5 as axons follow the differentiating arteries and continue to branch throughout development

(A) Pan-neuronal labeling (TUBB3, green) of an E12.5 urogenital system (UGS) shows that nerves are absent in the kidney (branching ureteric tree, cytokeratin, yellow). Ganglion and some postganglionic nerve fibers track along the descending aorta, shown by α-smooth muscle actin (αSMA; magenta). Scale bars: 300 μm and 100 μm (magnification)

(B) An E13.5 UGS shows that axons (TUBB3, green) innervate the kidney following the αSMA^{+} vascular mural cells (magenta) of the developing arteries (arrowheads, magnified

image). CD31 (yellow) labels the endothelial network. Scale bars: 300 μm and 100 μm (magnification).

(C) Axons (TUBB3, green) continue to grow and branch following the developing arterial tree (αSMA, magenta) at E16.5. Cytokeratin (yellow) marks the collecting duct system. Multiple axon bundles can be observed on an artery (arrowhead, magnified image). Scale bars: 250 μm and 90 μm (magnification).

(D) By E18.5, axons (TUBB3, green) have undergone extensive growth with the arterial tree (αSMA, magenta) and interstitial branching as the nerves navigate toward and around kidney structures like glomeruli (podocin, yellow; arrowhead, magnified image). Scale bars: 400 μm and 50 μm (magnification).

All images are representative of a minimum of 3 mice. See also Figure S1 and Videos S1, S2, S3, S4, and S5.

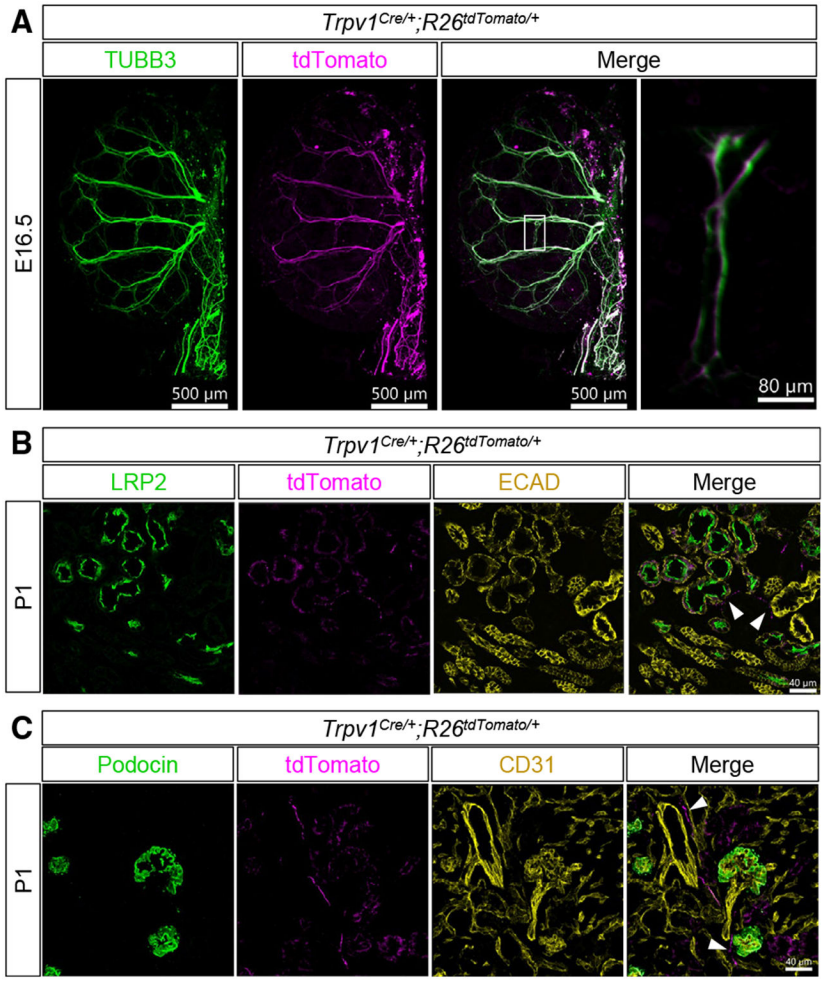

Figure 2. Nociceptive sensory afferent nerves innervate the developing kidney

(A) E16.5 *Trpv1*$^{Cre/+}$;*R26*$^{tdTomato/+}$ kidney showing tdTomato^{+} (magenta) axons colocalizing with TUBB3 (green). A magnified inset from the merge shows tdTomato^{+} axons overlapping with TUBB3. Scale bars: 500 μm and 80 μm (magnification).

(B) *Trpv1*$^{Cre/+}$;*R26*$^{tdTomato/+}$ P1 kidney section showing the tdTomato signal (magenta) closely associating (arrowheads) with proximal tubules (LRP2, green) and tubule epithelium (ECAD, yellow). Scale bar: 40 μm.

(C) *Trpv1*$^{Cre/+}$;*R26*$^{tdTomato/+}$ P1 kidney section showing the tdTomato signal (magenta) closely associating (arrowheads) with glomeruli (podocin, green) and endothelium (CD31, yellow).

Tubules in (B) and (C) show a non-specific tdTomato signal. Scale bar: 40 μm. All images are representative of a minimum of 3 mice.

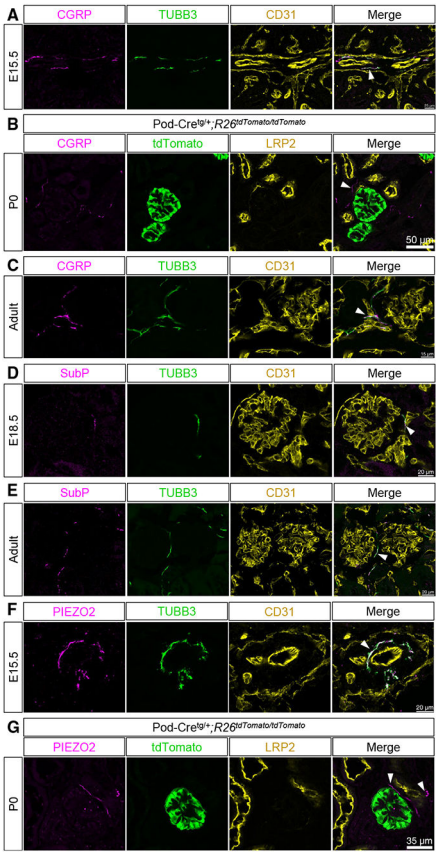

Figure 3. Peptidergic and mechanosensory afferent nerves are present in the developing kidney

(A) E15.5 kidney sections show that CGRP^{+} (magenta) axons (TUBB3, green) are mainly associated with the kidney vasculature (CD31, yellow; arrowhead) at this stage. Scale bar: 25 µm.

(B) Sections of Pod-Cre$^{tg/+}$;*R26*$^{tdTomato/tdTomato}$ P0 kidneys show CGRP^{+} axons (magenta) near (arrowhead) glomeruli (tdTomato, green) and close to proximal tubules (LRP2, yellow). Scale bar: 50 µm.

(C) Adult kidney section shows CGRP^{+} (magenta) axons colocalized with TUBB3 (green) closely associating with the vasculature (CD31, yellow) and near glomeruli (arrowhead). Scale bar: 15 µm.

(D) E18.5 kidney sections show substance P (SubP; magenta) overlap with TUBB3 (green) and associations with the vasculature (CD31, yellow) and glomeruli (arrowhead). Scale bar = 20 µm.

(E) Adult kidney section shows SubP^{+} (magenta) axons (TUBB3, green) along the vasculature (CD31, yellow) and in close proximity to glomeruli (arrowhead). Scale bar: 20 µm.

(F) E15.5 kidney section shows PIEZO2^{+} (magenta) axons (TUBB3, green) associating with the vasculature (CD31, yellow; arrowhead). Scale bar: 20 µm.

(G) Sections of Pod-Cre$^{tg/+}$;*R26*$^{tdTomato/tdTomato}$ P0 kidneys show PIEZO2^{+} nerves (magenta) closely associating (arrowheads) with glomeruli (tdTomato, green) and proximal tubules (LRP2, yellow). Scale bar: 35 µm.

All images are representative of a minimum of 3 mice. See also Figures S2 and S3.

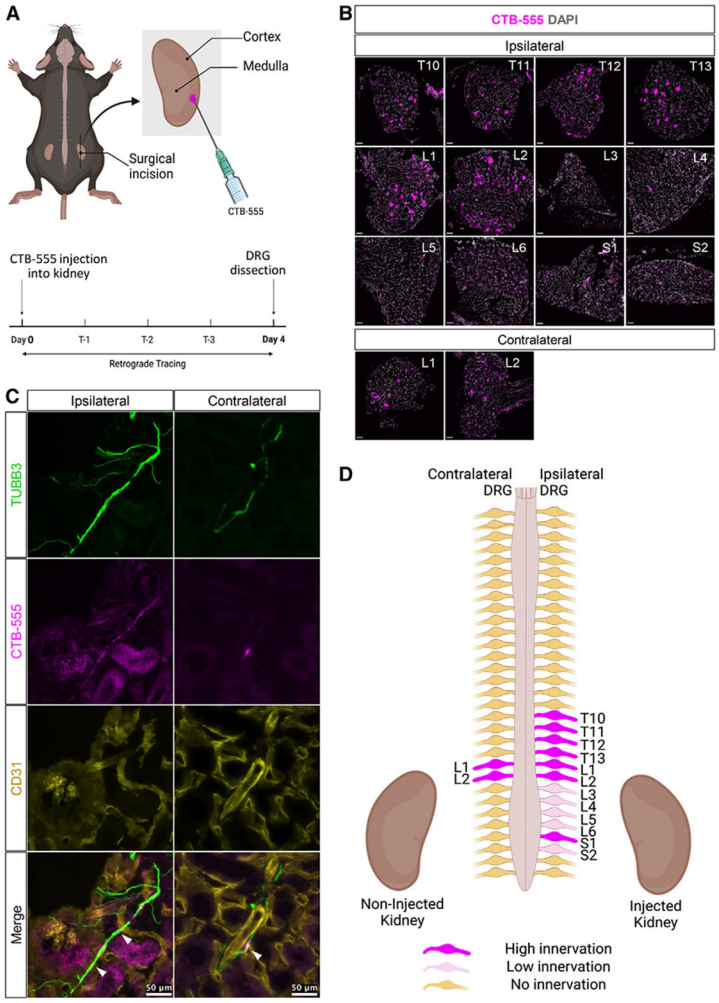

Figure 4. CTB retrograde tracing shows axon trajectories and labeling of thoracic, lumbar, and sacral DRG

(A) Schematic of CTB-555 retrograde tracing and timeline (created with BioRender).

(B) Sensory innervation primarily traces in the ipsilateral DRG to the lower thoracic (T10–T13), lumbar (L1–6), and sacral (S1–S2) regions. Tracing to the contralateral DRG was observed in the upper lumbar region of L1 and L2. $n = 4$ males and $n = 4$ females. Scale bars: 50 µm.

(C) Ipsilateral and contralateral kidney sections of a CTB-injected mouse. The ipsilateral kidney section shows CTB^+ (magenta) axons colocalizing with TUBB3 (green) near glomeruli and vasculature (CD31, yellow; arrowheads). CTB (magenta) colocalized with TUBB3 (green) near vasculature (CD31, yellow; arrowhead) in the contralateral kidney. Scale bars: 50 µm.

(D) Schematic of the spinal level and DRG origin of kidney sensory afferent innervation (created with BioRender.

See also Figure S3.

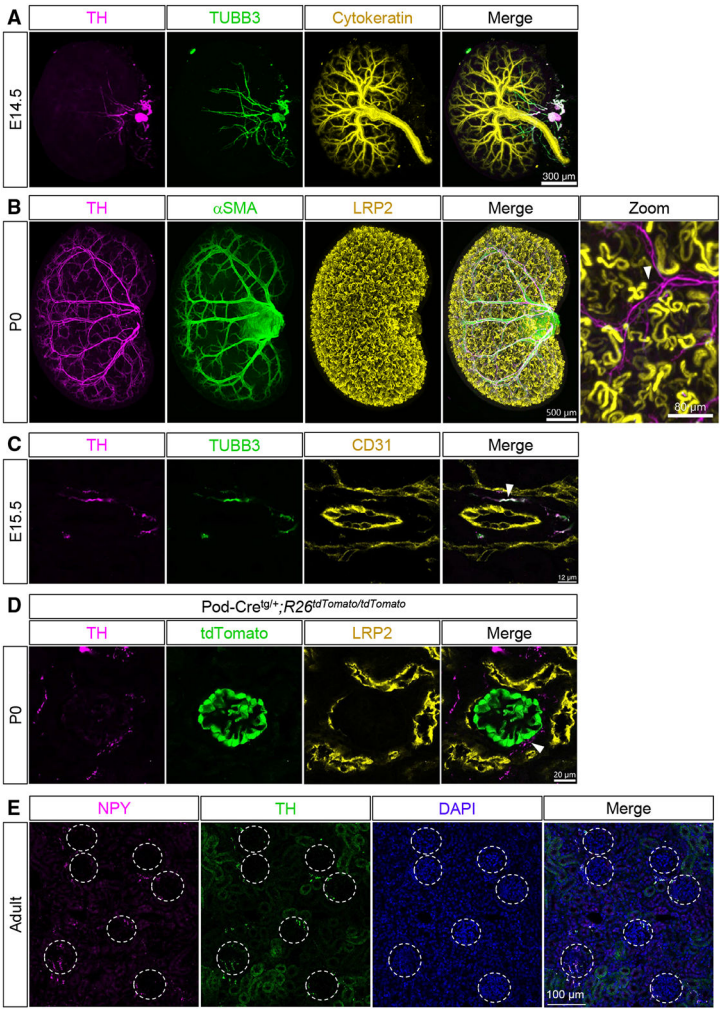

Figure 5. Noradrenergic sympathetic nerves innervate the developing kidney

(A) E14.5 kidney labeled with tyrosine hydroxylase (TH; magenta) shows that the first innervating axons (TUBB3, green) are TH^+. Cytokeratin (yellow) marks the developing collecting duct system. Scale bars: 300 μm.

(B) P0 kidney labeled with TH (magenta) shows that the TH^+ nerves have branched extensively alongside the arterial tree (αSMA, green). LRP2 marks the proximal tubules (yellow), and the magnified inset shows TH^+ nerves (magenta) navigating around and near proximal tubules (arrowhead). Scale bars: 500 μm and 80 μm (magnification).

(C) E15.5 kidney section showing TH^+ axons (TH, magenta; TUBB3, green) around the vasculature (CD31, yellow; arrowhead). Scale bar: 12 μm.

(D) Sections of Pod-$Cre^{tg/+}$;*R26*$^{tdTomato/tdTomato}$ P0 kidneys show TH^+ axons (magenta) near glomeruli (tdTomato, green; arrowhead) and proximal tubules (LRP2, yellow). Scale bar: 20 μm.

(E) Adult kidney cortex immunostained for neuropeptide Y (NPY; magenta), TH (green), and DAPI (blue). Glomeruli are encircled (white dotted lines). No TH^+/NPY^- fibers were observed. Scale bar: 100 μm.

The image (E) is representative of 2 male mice; the images in (A)–(D) are representative of a minimum of 3 mice. See also Figures S4 and S5.

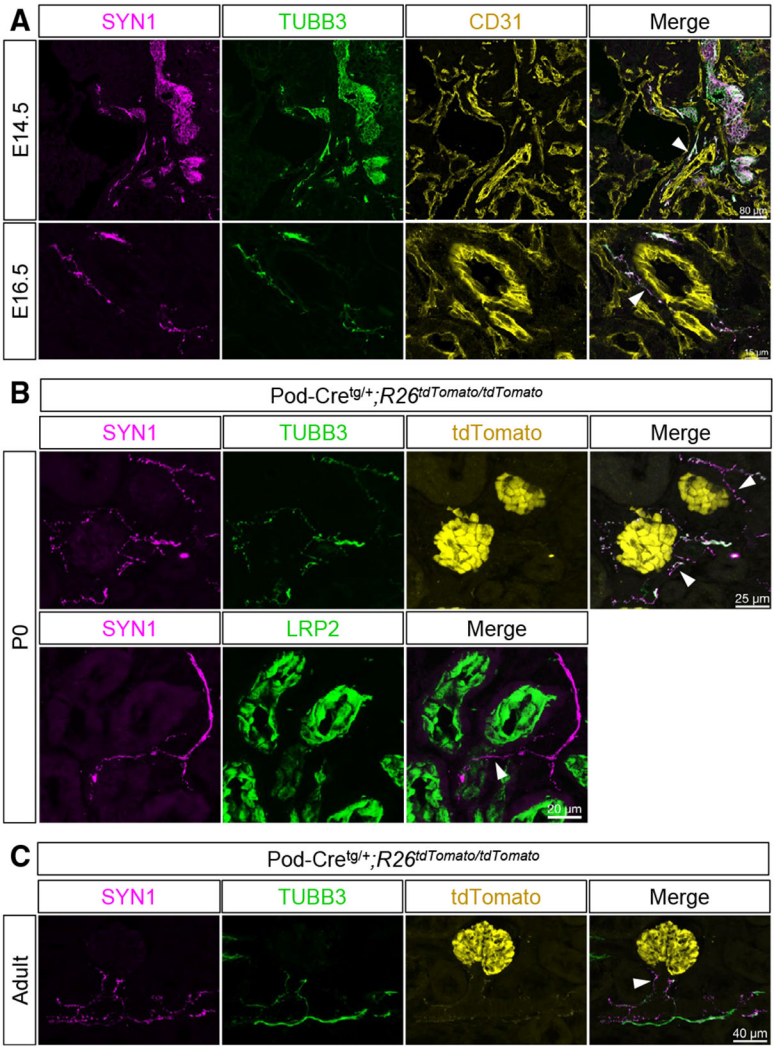

Figure 6. SYN1^{+} nerves highlight the potential for neuroeffector-junction formation during kidney development

(A) Top: E14.5 kidney sections show overlap of synapsin I (SYN1, magenta) with TUBB3 (green) and association of axons with the main artery (CD31, yellow; arrowhead). Scale bar: 80 µm. Bottom: E16.5 kidney sections similarly show SYN1^{+} (magenta) and TUBB3^{+} (green) nerves around the vasculature (CD31, yellow; arrowhead). Scale bar: 15 µm.

(B) Sections of Pod-Cre$^{tg/+}$;$R26^{tdTomato/tdTomato}$ P0 kidneys show SYN1^{+} axons (magenta) overlapping with TUBB3 (green) near glomeruli (tdTomato, yellow; arrowheads, top) and proximal tubules (LRP2, green; arrowhead, bottom). Scale bars: 25 µm (top) and 20 µm (bottom).

(C) Sections of Pod-Cre$^{tg/+}$;$R26^{tdTomato/tdTomato}$ adult kidneys show SYN1^{+} (magenta) and TUBB3^{+} (green) axons along the arterioles near glomeruli (tdTomato, yellow; arrowhead). Scale bar = 40µm. All images are representative of a minimum of n = 3 mice.

See also Figure S6.

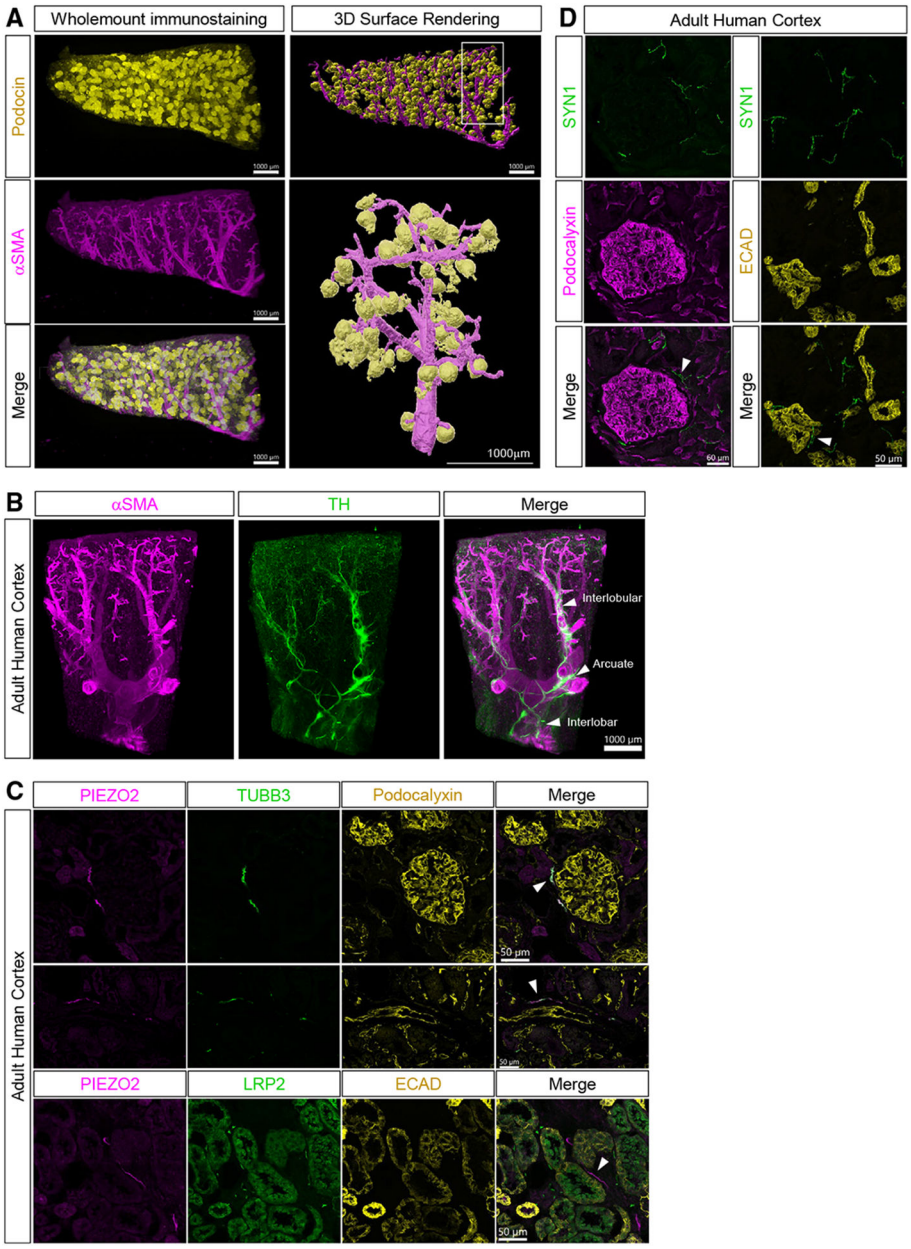

Figure 7. Sympathetic and sensory nerves show similar structural associations in the adult human kidney

(A) Human kidney cortex labeled with podocin (yellow) and αSMA (magenta), showing interlobular arteries branching and glomerular organization (magnified 3D rendering). Scale bars: 1,000 μm.

(B) Human kidney cortex labeled with TH (green) and αSMA (magenta), showing sympathetic nerves branching with interlobar, arcuate, and interlobular arteries (arrowheads). Scale bar: 1,000 μm.

(C) Adult human kidney cortical sections show PIEZO2 (magenta) overlapping with TUBB3 (green) and associating with glomeruli (podocalyxin, yellow; arrowhead, top), vasculature

(podocalyxin, yellow; arrowhead, center), and near epithelial structures (LRP2, green; ECAD, yellow; arrowhead, bottom). Scale bars: 50 μm.

(D) Adult human kidney cortical sections show $SYN1^+$ axons (green) near glomeruli (podocalyxin, magenta; arrowhead, left) and epithelial structures (ECAD, yellow; arrowhead, right). Scale bars: 60 μm (left) and 50 μm (right).

All images are representative of tissue acquired from two human samples. See also Figure S7 and Videos S6, S7, and S8.

KEY RESOURCES TABLE

REAGENT or RESOURCE	SOURCE	IDENTIFIER
Antibodies		
TUBB3; Mouse IgG2a; Section IF: 1:500, Wholemount IF: 1:250	BioLegend	Cat#801202; RRID:AB_2313773
TUBB3-594; Mouse IgG2a; Section IF: 1:500, Wholemount IF: 1:250	BioLegend	Cat#801208; RRID:AB_2650636
Neurofilament (NFH); Chicken; Section IF: 1:1000	Abcam	Cat#ab4680; RRID:AB_304560
Tyrosine Hydroxylase (TH); Rabbit; Section IF: 1:500, Wholemount IF: 1:250	Invitrogen/Thermo Fisher Scientific	Cat#OPA1-04050; RRID:AB_325653
Tyrosine Hydroxylase (TH); Chicken; Section IF: 1:250	Abcam	Cat#ab76442; RRID:AB_1524535
Neuropeptide Y (NPY); Chicken; Section IF: 1:250	Novus Biologicals	Cat#NBP1-46535; RRID:AB_10009813
CGRP; Rabbit; Section IF: 1:250	Immunostar	Cat#24112; RRID:AB_572217
CGRP; Mouse IgG2a; Section IF: 1:250	Abcam	Cat#ab81887; RRID:AB_1658411
PIEZO2; Rabbit; Section IF: 1:250, Wholemount IF: 1:250	Novus Biologicals	Cat#NBP1-78624; RRID:AB_11005294
PIEZO2; Rabbit; Section IF: 1:250, Wholemount IF: 1:250	Novus Biologicals	Cat#NBP1-78538; RRID:AB_11031775
Substance P (SubP); Rabbit; Section IF: 1:100	Immunostar	Cat#20064; RRID:AB_572266
Synapsin 1 (SYN1); Rabbit; Section IF: 1:1000	Invitrogen/Thermo Fisher Scientific	Cat#51-5200; RRID:AB_2533909
VAChT; Rabbit; Section IF: 1:250	Synaptic Systems	Cat#139103; RRID:AB_887864
VAChT; Guinea Pig; Section IF: 1:100	Synaptic Systems	Cat#139105; RRID:AB_10893979
RFP; Chicken; Section IF: 1:500, Wholemount IF: 1:250	Rockland	Cat#600-901-379; RRID:AB_10704808
RFP; Rabbit; Section IF: 1:500, Wholemount IF: 1:250	Rockland	Cat#600-401-379; RRID:AB_2209751
αSMA-488; Mouse IgG2a; Section IF: 1:500, Wholemount IF: 1:250	Invitrogen/Thermo Fisher Scientific	Cat#53-9760-82; RRID:AB_2574461
Podocin (NPHS2); Rabbit; Section IF: 1:500, Wholemount IF: 1:250	Invitrogen/Thermo Fisher Scientific	Cat#PA579757; RRID:AB_2746872
Cytokeratin; Mouse IgG1; Section IF: 1:500, Wholemount IF: 1:250	Sigma-Aldrich	Cat#C2931; RRID:AB_258824
Megalin (LRP2); Mouse IgG1; Section IF: 1:500, Wholemount IF: 1:250	MyBiosource	Cat#MBS690201
E-cadherin (ECAD); Rat; Section IF: 1:500, Wholemount IF: 1:250	Invitrogen/Thermo Fisher Scientific	Cat#13-1900; RRID:AB_2533005
CD31; Rat; Section IF: 1:100, Wholemount IF: 1:50	BD Pharmingen	Cat#550274; RRID:AB_393571
Podocalyxin (PODXL); Goat; Section IF: 1:500, Wholemount IF: 1:250	R&D Systems	Cat#AF1658; RRID:AB_354920
Bacterial and virus strains		
pAAV-FLEX-tdTomato	Chan et al.[43]	Addgene 28306; RRID:Addgene_28306
Biological samples		
De-identified human kidney tissue	University of North Carolina at Chapel Hill Tissue Procurement Facility	https://unclineberger.org/tissue-procurement/
Chemicals, peptides, and recombinant proteins		
Cholera Toxin Subunit B-555 (Recombinant)	Invitrogen	C34776

REAGENT or RESOURCE	SOURCE	IDENTIFIER
32% Paraformaldehyde (formaldehyde) aqueous solution	Electron Microscopy Sciences	15714
Methanol	Fisher Scientific	A433P-4
CHAPS hydrate	Sigma	C3023
Dichloromethane	Sigma	270997
Dibenzyl Ether	Sigma	33630
Agarose	Fisher	BP160-500
Heparin	Sigma-Aldrich	H4784
Sheep Serum	Gibco	16070096
Donkey Serum	Equitech-Bio	SD30-0100
Normal donkey serum	Sigma-Aldrich	D9663
Normal goat serum	Life Technologies	PCN5000
Bovine Serum Albumin (BSA)	Fisher	BP9706-100
Triton X-100	Fisher	BP151-500
DirectPCR Lysis buffer	Viagen Biogen	102-T
10x PBS pH 7.4	Gibco	70011044
Sucrose	Fisher	S5-500
Tissue-Plus O.C.T. Compound	Fisher	23-730-571
Tissue-Tek O.C.T	Sakura	4583
VectaShield	Vector Laboratories	H-1000-10
ProLong Gold Antifade Mountant	Thermo Fisher Scientific	P36930
Fluoromount-G Mounting Medium, with DAPI	Thermo Fisher Scientific	00-4959-52
Deposited data		
Imaging files	UNC Dataverse	https://dataverse.unc.edu/dataverse/D_24_01486_obrienlab
Experimental models: organisms/strains		
Swiss Webster	Taconic Biosciences	Tac:SW; RRID:IMSR_TAC:SW
C57BL/6J	Jackson Labs	Strain #:000664; RRID:IMSR_JAX:000664
B6.129-Trpv1tm1(cre)Bbm/J (Trpv1$^{Cre/+}$)	Jackson Labs	Strain #:017769; RRID:IMSR_JAX:017769
B6.Cg-Tg(NPHS2-cre)295Lbh/J (Pod-Cre^{ig})	Jackson Labs	Strain #:008205; RRID:IMSR_JAX:008205
B6(SJL)-Piezo2tm1.1(cre)Apat/J (Piezo2$^{EGFP-IRES-Cre}$)	Jackson Labs	Strain #:027719; RRID:IMSR_JAX:027719
B6.Cg-Gt(ROSA)26Sortm14(CAG-tdTomato)Hze/J (R26^{tdTomato})	Jackson Labs	Strain #:007914; RRID:IMSR_JAX:007914
Oligonucleotides		
Primers for genotyping, see Table S1	This paper	N/A
Software and algorithms		
Imaris ×64 v9.9.1	Oxford Instruments	N/A
Imaris file converter v9.8.2	Oxford Instruments	N/A
Imaris sticher v9.9.1	Oxford Instruments	N/A
Fiji	https://imagej.net/software/fiji/	N/A
Prism	https://www.graphpad.com/	N/A

REAGENT or RESOURCE	SOURCE	IDENTIFIER
R	https://www.r-project.org/	N/A
ggplot2	https://cran.r-project.org/web/packages/ggplot2/index.html	N/A
ComplexHeatmap	http://www.bioconductor.org/packages/devel/bioc/html/ComplexHeatmap.html	N/A